

1 **Humans strategically shift decision bias by flexibly**
2 **adjusting sensory evidence accumulation in visual cortex**

3

4 Niels A. Kloosterman^{*1,2}, Jan Willem de Gee³, Markus Werkle-Bergner², Ulman
5 Lindenberger^{1,2}, Douglas D. Garrett^{1,2+}, Johannes Jacobus Fahrenfort^{4,5+}

6

7 ¹ Max Planck UCL Centre for Computational Psychiatry and Ageing Research, Max Planck Institute
8 for Human Development, Lentzeallee 94, 14195 Berlin, Germany

9 ² Center for Lifespan Psychology, Max Planck Institute for Human Development, Lentzeallee 94,
10 14195 Berlin, Germany

11 ³ Department of Neurophysiology and Pathophysiology, University Medical Center Hamburg-
12 Eppendorf, Germany;

13 ⁴ Department of Psychology, University of Amsterdam, The Netherlands;

14 ⁵ Department of Experimental and Applied Psychology, Vrije Universiteit, van der Boechorststraat 1,
15 1081 BT Amsterdam, The Netherlands

16 *Shared senior author

17 *Correspondence: kloosterman@mpib-berlin.mpg.de

18

19 **Corresponding author information**

20 Niels A. Kloosterman, Ph.D.

21 Max Planck UCL Centre for Computational Psychiatry and Ageing Research,
22 Lentzeallee 94, 14195, Berlin, Germany

23 Phone: +49 30 82406 424

24 E-mail: kloosterman@mpib-berlin.mpg.de

25 **Abstract**

26 Decision bias is traditionally conceptualized as an internal reference against which
27 sensory evidence is compared. Here, we show that individuals are able to
28 strategically shift this internal reference depending on current task demands by
29 changing the rate of sensory evidence accumulation in visual cortex. Participants
30 performed a target detection task during EEG recordings. We experimentally
31 manipulated participants' decision criterion for reporting target-present using different
32 stimulus-response reward contingencies, inducing liberal and conservative biases in
33 different conditions. Drift diffusion modeling revealed that a strategic liberal bias shift
34 specifically biased sensory evidence accumulation towards target-present choices.
35 In visual cortex, the liberal bias suppressed pre-stimulus 8—12 Hz (alpha) power,
36 which in turn mediated output activity of visual cortex, as expressed in 59—100 Hz
37 (gamma) power. These findings show that observers can intentionally control cortical
38 excitability to strategically bias evidence accumulation towards the decision bound
39 that maximizes reward within a given ecological context.

40

41 **Introduction**

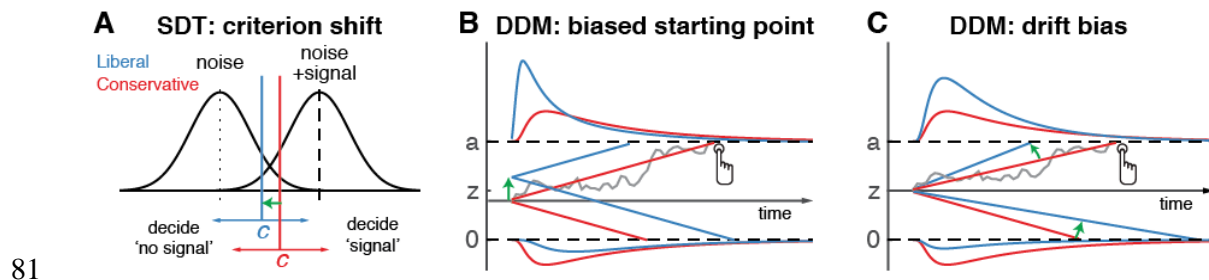
42 Perceptual decisions arise not only from the evaluation of sensory evidence, but are
43 often biased towards one or another choice alternative by environmental factors,
44 perhaps as a result of task instructions and/or stimulus-response reward
45 contingencies (White & Poldrack, 2014). The ability to willfully control decision bias
46 could potentially enable the behavioral flexibility required to survive in an ever-
47 changing and uncertain environment. But despite its important role in decision
48 making, the neural mechanisms underlying decision bias are not fully understood.

49 The traditional account of decision bias comes from signal detection theory
50 (SDT) (Green & Swets, 1966). In SDT, decision bias is quantified by estimating the

51 relative position of a decision point or ‘criterion’ in between sensory evidence
52 distributions for noise and signal (see Figure 1A). In this framework, a more liberal
53 decision bias arises by moving the criterion closer towards the noise distribution (see
54 green arrow in Figure 1A). Although SDT has been very successful at quantifying
55 decision bias, how exactly bias affects decision making and how it is reflected in
56 neural activity remains unknown.

57 One reason for this lack of insight may be that SDT does not have a temporal
58 component to track how decisions are reached over time (Fetsch, Kiani, & Shadlen,
59 2014). As an alternative to SDT, the drift diffusion model (DDM) conceptualizes
60 perceptual decision making as the accumulation of noisy sensory evidence over time
61 into an internal decision variable (Bogacz, Brown, Moehlis, Holmes, & Cohen, 2006;
62 Gold & Shadlen, 2007; Ratcliff & McKoon, 2008). A decision in this model is made
63 when the decision variable crosses one of two decision bounds corresponding to the
64 choice alternatives. After one of the bounds is reached, the corresponding decision
65 can subsequently either be actively reported, for example by means of a button
66 press indicating a detected signal, or it could remain without behavioral report when
67 no signal is detected (Ratcliff, Huang-Pollock, & McKoon, 2016). Within this
68 framework, a strategic decision bias imposed by the environment can be modelled in
69 two different ways: either by moving the starting point of evidence accumulation
70 closer to one of the boundaries (see green arrow in Figure 1B), or by biasing the rate
71 of the evidence accumulation process itself towards one of the boundaries (see
72 green arrow in Figure 1C). In both the SDT and DDM frameworks, decision bias
73 shifts have little effect on the sensitivity of the observer when distinguishing signal
74 from noise; they predominantly affect the relative response ratios (and in the case of
75 DDM the speed with which one or the other decision bound is reached). There has

76 been some evidence to suggest that decision bias induced by shifting the criterion is
77 best characterized by a drift bias in the DDM (Urai, de Gee, & Donner, 2018; White &
78 Poldrack, 2014). However, the drift bias parameter has as yet not been related to a
79 well-described neural mechanism.
80



82 **Figure 1 | Theoretical accounts of decision bias.** **A.** Signal-detection-theoretic account of decision
83 bias. Signal and noise+signal distributions are plotted as a function of the strength of internal sensory
84 evidence. The decision point (or criterion) that determines whether to decide signal presence or
85 absence is plotted as a vertical criterion line c , reflecting the degree of decision bias. c can be shifted
86 left- or rightwards to denote a more liberal or conservative bias, respectively (green arrow indicates a
87 shift towards more liberal). **B, C:** Drift diffusion model (DDM) account of decision bias, in which
88 decisions are modelled in terms of a set of parameters that describe a dynamic process of sensory
89 evidence accumulation towards one of two decision bounds. When sensory input is presented,
90 evidence starts to accumulate (drift) over time after initialization at the starting point z . A decision is
91 made when the accumulated evidence either crosses decision boundary a (signal presence) or
92 decision boundary 0 (no signal). After a boundary is reached, the corresponding decision can be
93 either actively reported by a button press (e.g. for signal-present decisions), or remain implicit, without
94 a response (for signal-absent decisions). The DDM can capture decision bias through a shift of the
95 starting point of the evidence accumulation process (panel B) or through a shift in bias in the rate of
96 evidence accumulation towards the different choices (panel C). These mechanisms are dissociable
97 through their differential effect on the shape of the reaction time (RT) distributions, as indicated by the
98 curves above and below the graphs for target-present and target-absent decisions, respectively.
99 Panels B. and C. are modified and reproduced with permission from Urai, de Gee, & Donner (2018).

100

101 Regarding the neural underpinnings of decision bias, there have been a
102 number of reports about a correlational relationship between cortical population
103 activity measured with EEG and decision bias. For example, spontaneous trial-to-
104 trial variations in pre-stimulus oscillatory activity in the 8—12 Hz (alpha) band have
105 been shown to correlate with decision bias and confidence (Iemi, Chaumon, Crouzet,
106 & Busch, 2017; Limbach & Corballis, 2016; Samaha, Iemi, & Postle, 2017). Alpha
107 oscillations, in turn, have been proposed to be involved in the gating of task-relevant
108 sensory information (Jensen & Mazaheri, 2010), possibly encoded in high-frequency
109 (gamma) oscillations in visual cortex (Ni et al., 2016; Popov, Kastner, & Jensen,
110 2017). Although these reports suggest links between pre-stimulus alpha
111 suppression, sensory information gating and decision bias, they do not uncover
112 whether pre-stimulus alpha plays an instrumental role in decision bias and how
113 exactly this might be achieved. For example, it is unknown whether an
114 experimentally induced shift in decision bias is implemented in the brain by willfully
115 adjusting pre-stimulus alpha in sensory areas.

116 Here, we explicitly investigate these potential mechanisms by employing a
117 task paradigm in which shifts in decision bias were experimentally induced within
118 participants through (a) instruction and (b) asymmetries in stimulus-response reward
119 contingencies during a visual target detection task. By applying drift diffusion
120 modeling to the participants' choice behavior, we show that strategically adjusting
121 decision bias specifically affects the rate of sensory evidence accumulation towards
122 one of the two decision bounds. Further, we demonstrate that this drift bias is
123 achieved by flexibly up- and down-regulating pre-stimulus alpha as well as the output
124 activity of visual cortex, as reflected in gamma power modulation. Critically, we show

125 that gamma activity accurately predicts the strength of the evidence accumulation
126 bias within participants, providing a direct link between the proposed mechanism and
127 decision bias. Together, these findings identify the neural mechanism by which
128 intentional control of cortical excitability is applied to strategically bias perceptual
129 decisions in order to maximize reward in a given context.

130

131 **Results**

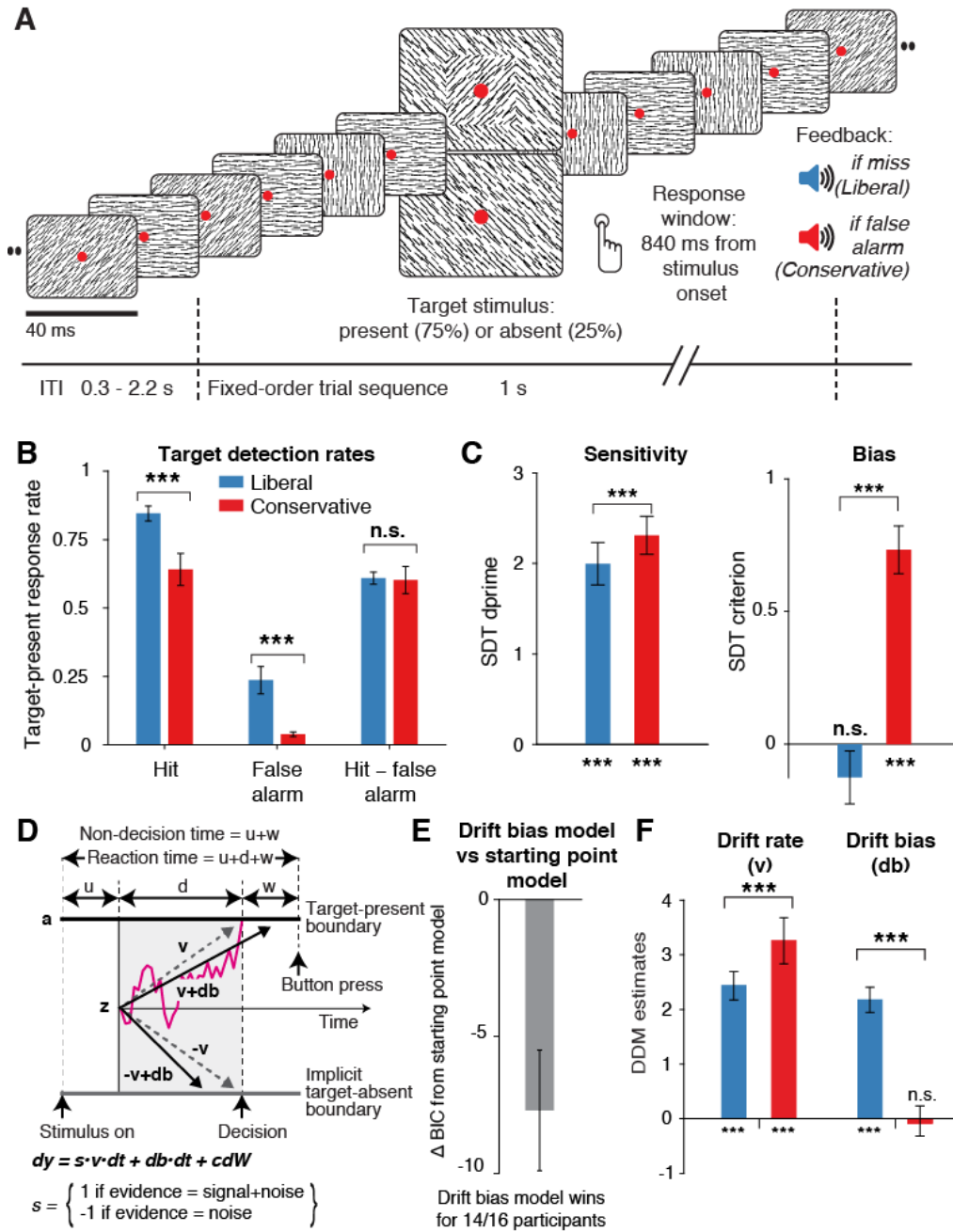
132 **Manipulation of decision bias affects sensory evidence accumulation**

133 In three EEG recording sessions, human participants (N = 16) viewed a continuous
134 stream of horizontal, vertical and diagonal line textures alternating at a rate of 25
135 textures/second. The participants' task was to detect an orientation-defined square
136 presented in the center of the screen and report it via a button press (Figure 2A).
137 Trials consisted of a fixed-order sequence of textures embedded in the continuous
138 stream (total sequence duration 1 second). A square appeared in the fifth texture of
139 a trial in 75% of the presentations (target trials), while in 25% a homogenous
140 diagonal texture appeared in the fifth position (nontarget trials). Although the onset of
141 a trial within the continuous stream of textures was not explicitly cued, the similar
142 distribution of reaction times in target and nontarget trials suggests that participants
143 used the temporal structure of the task even when no target appeared (Figure 2—
144 figure supplement 1A). Consistent and significant EEG power modulations after trial
145 onset (even for nontarget trials) further confirm that subjects registered trial onsets in
146 the absence of an explicit cue, plausibly using the onset of a fixed order texture
147 sequence as an implicit cue (Figure 2—figure supplement 1B).

148 In alternating nine-minute blocks of trials, we actively biased participants'
149 perceptual decisions by instructing them either to report as many targets as possible
150 (“Detect as many targets as possible!”; liberal condition), or to only report high-
151 certainty targets (“Press only if you are really certain!”; conservative condition).
152 Participants were free to respond at any time during a block whenever they detected
153 a target. A trial was considered a target present response when a button press
154 occurred before the fixed-order sequence ended (i.e. within 0.84 s after onset of the
155 fifth texture containing the (non)target, see Figure 2A). We provided auditory
156 feedback and applied monetary penalties following missed targets in the liberal
157 condition and following false alarms in the conservative condition (Figure 2A; see
158 Methods for details). The median number of trials for each SDT category across
159 participants was 1206 hits, 65 false alarms, 186 misses and 355 correct rejections in
160 the liberal condition, and 980 hits, 12 false alarms, 419 misses and 492 correct
161 rejections in the conservative condition.

162 Participants reliably adopted the intended decision bias shift across the two
163 conditions, as shown by both the hit rate and the false alarm rate going down in
164 tandem as a consequence of a more conservative bias (Figure 2B). The difference
165 between hit rate and false alarm rate was not significantly modulated by the
166 experimental bias manipulations ($p = 0.81$, two-sided permutation test, 10,000
167 permutations, see Figure 2B). However, target detection performance computed
168 using standard SDT d' (perceptual sensitivity, reflecting the distance between the
169 noise and signal distributions in Figure 1A)(Green & Swets, 1966) was slightly higher
170 during conservative (liberal: $d' = 2.0$ (s.d. 0.90), versus conservative: $d' = 2.31$ (s.d.
171 0.82), $p = 0.0002$, see Figure 2C, left bars). We quantified decision bias using the
172 standard SDT criterion measure c , in which positive and negative values reflect

173 conservative and liberal biases, respectively (see the blue and red vertical lines in
 174 Figure 1A). This uncovered a strong experimentally induced bias shift from the
 175 conservative to the liberal condition (liberal: $c = -0.13$ (s.d. 0.4), versus
 176 conservative: $c = 0.73$ (s.d. 0.36), $p = 0.0001$, see Figure 2C), as well as a
 177 conservative average bias across the two conditions ($c = 0.3$ (s.d. 0.31), $p = 0.0013$).



178

179 **Figure 2 | Strategic decision bias shift towards liberal biases evidence accumulation. A.**
180 Schematic of the visual stimulus and task design. Participants viewed a continuous stream of full-
181 screen diagonally, horizontally and vertically oriented textures at a presentation rate of 40 ms (25 Hz).
182 After random inter-trial intervals (range 0.3—2.2 s), a fixed-order sequence (duration 1 s) was
183 presented, embedded in the stream. The fifth texture in each sequence either consisted of a single
184 diagonal orientation (target absent), or contained an orthogonal orientation-defined square (either 45°
185 or 135° orientation). Participants decided whether they had just seen a target, reporting detected
186 targets by button press within 840 ms after target onset. Liberal and conservative conditions were
187 administered in alternating nine-minute blocks by penalizing either misses or false alarms,
188 respectively, using aversive tones and monetary deductions. Depicted square and fixation dot sizes
189 are not to scale. **B.** Average detection rates (hits and false alarms) during both conditions. Miss rate is
190 equal to 1 – hit rate since both are computed on stimulus present trials, and correct-rejection rate as 1
191 – false alarm rate since both are computed on stimulus absent trials, together yielding the four SDT
192 stimulus-response categories **C.** SDT parameters for sensitivity and criterion. **D.** Schematic and
193 simplified equation of drift diffusion model accounting for reaction time distributions for actively
194 reported target-present and implicit target-absent decisions. Decision bias in this model can be
195 implemented by either shifting the starting point of the evidence accumulation process (Z), or by
196 adding an evidence-independent constant ('drift bias', db) to the drift rate. See text and Figure 1 for
197 details. Notation: dy , change in decision variable y per unit time dt ; $v \cdot dt$, mean drift (multiplied with 1
198 for signal + noise (target) trials, and -1 for noise-only (nontarget) trials); $db \cdot dt$, drift bias; and cdW ,
199 Gaussian white noise (mean = 0, variance = $c^2 \cdot dt$). **E.** Difference in Bayesian Information Criterion
200 (BIC) goodness of fit estimates for the drift bias and the starting point models. A lower delta BIC value
201 indicates a better fit, showing superiority of the drift bias model to account for the observed results. **F.**
202 Estimated model parameters for drift rate and drift bias in the drift bias model. Error bars, SEM across
203 16 participants. *** $p < 0.001$; n.s., not significant. Panel D. is modified and reproduced with
204 permission from (de Gee et al., 2017).

205 The following source data and figure supplements are available for Figure 2:

206 **Source data 1.** This csv table contains the data for Figure 2 panels B, C, E and F.

207 **Figure supplement 1.** Behavioral and neurophysiological evidence that participants were sensitive to
208 the implicit task structure.

209 **Figure supplement 2.** Signal-detection-theoretic behavioral measures during both conditions
210 correspond closely to drift diffusion modeling parameters.

211 **Figure supplement 3.** Single-participant drift diffusion model fits for the drift bias model for both
212 conditions.

213 Because the SDT framework is static, we further investigated how bias
214 affected various components of the dynamic decision process by fitting different drift
215 diffusion models (DDMs) to the behavioral data (Figure 1B, C) (Ratcliff & McKoon,
216 2008). The DDM postulates that perceptual decisions are reached by accumulating
217 noisy sensory evidence towards one of two decision boundaries representing the
218 choice alternatives. Crossing one of these boundaries can either trigger an explicit
219 behavioral report to indicate the decision (for target-present responses in our
220 experiment), or remain implicit (i.e. without active response, for target-absent
221 decisions in our experiment). The DDM captures the dynamic decision process by
222 estimating parameters reflecting the rate of evidence accumulation (drift rate), the
223 separation between the boundaries, as well as the time needed for stimulus
224 encoding and response execution (non-decision time)(Ratcliff & McKoon, 2008). The
225 DDM is able to estimate these parameters based on the shape of the RT
226 distributions for actively reported (target-present) decisions along with the total
227 number of trials in which no response occurred (i.e. implicit target-absent decisions)
228 (Ratcliff et al., 2016).

229 We tested two different DDMs that can potentially account for decision bias:
230 one in which the starting point of evidence accumulation moves closer to one of the
231 decision boundaries ('starting point model', Figure 1B) (Mulder, Wagenmakers,
232 Ratcliff, Boekel, & Forstmann, 2012), and one in which the drift rate itself is biased
233 towards one of the boundaries (de Gee et al., 2017) ('drift bias model', see Figure

234 1C, referred to as drift criterion by Ratcliff and McKoon (2008)). The drift bias
235 parameter is determined by estimating the contribution of an evidence-independent
236 constant added to the drift (Figure 2D). In the two respective models, we freed either
237 the drift bias parameter (db , see Figure 2D) for the two conditions while keeping
238 starting point (z) fixed across conditions (for the drift bias model), or vice versa (for
239 the starting point model). Permitting only one parameter at a time to vary freely
240 between conditions allowed us to directly compare the models without having to
241 penalize either model for the number of free parameters. These alternative models
242 make different predictions about the shape of the RT distributions in combination
243 with the response ratios: a shift in starting point results in more target-present
244 choices particularly for short RTs, whereas a shift in drift bias grows over time,
245 resulting in more target-present choices also for longer RTs (de Gee et al., 2017;
246 Ratcliff & McKoon, 2008; Urai et al., 2018). The RT distributions above and below
247 the evidence accumulation graphs in Figure 1B and 1C illustrate these different
248 effects. In both models, all of the non-bias related parameters (drift rate v , boundary
249 separation a and non-decision time $u+w$, see Figure 2D) were also allowed to vary
250 by condition.

251 We found that the starting point model provided a worse fit to the data than
252 the drift bias model (starting point model, Bayesian Information Criterion (BIC) =
253 10287; drift bias model, BIC = 10279, Figure 2E, see Methods for details).
254 Specifically, for 14 out of the 16 participants, the drift bias model provided a better fit
255 than the starting point model, for 10 of which $\Delta BIC > 6$, indicating strong
256 evidence in favor of the drift bias model. Finally, we compared these models to a
257 model in which both drift bias and starting point were fixed across the conditions,
258 while still allowing the non-bias-related parameters to vary per condition. This model

259 provided the lowest goodness of fit (delta BIC > 6 for both models for all
260 participants). See Figure 2—figure supplement 3 for model fits of the drift bias model
261 for each participant.

262 Given the superior performance of the drift bias model, we further
263 characterized decision making under the bias manipulation using parameter
264 estimates from this model. Drift rate, reflecting the participants' ability to discriminate
265 targets and nontargets, was somewhat higher in the conservative compared to the
266 liberal condition (liberal: $v = 2.39$ (s.d. 1.07), versus conservative: $v = 3.06$ (s.d.
267 1.16), $p = 0.0001$, permutation test, Figure 2F, left bars). Almost perfect correlations
268 across participants in both conditions between DDM drift rate and SDT d' provided
269 strong evidence that the drift rate parameter captures perceptual sensitivity (liberal, r
270 $= 0.97$, $p = 1.7e^{-10}$; conservative, $r = 0.95$, $p = 1.4e^{-8}$, see Figure 2—figure
271 supplement 2A).

272 Regarding the DDM bias parameters, the condition-fixed starting point
273 parameter in the drift bias model was smaller than half the boundary separation (i.e.
274 closer to the target-absent boundary ($z = 0.24$ (s.d. 0.06), $p < 0.0001$, tested against
275 0.5)), indicating an overall conservative starting point across conditions (Figure 2—
276 figure supplement 2D), in line with the overall positive SDT criterion (see Figure 2C,
277 right panel). Strikingly, however, whereas the drift bias parameter was on average
278 not different from zero in the conservative condition ($db = -0.04$ (s.d. 1.17), $p =$
279 0.90), drift bias was strongly positive in the liberal condition ($db = 2.08$ (s.d. 1.0), $p =$
280 0.0001 ; liberal vs conservative: $p = 0.0005$; Figure 2F, right bars). The overall
281 conservative starting point combined with a condition-specific neutral drift bias
282 explained the conservative decision bias (as quantified by SDT criterion) in the
283 conservative condition (Figure 2C). Likewise, in the liberal condition, the overall

284 conservative starting point combined with a condition-specific positive drift bias
285 (pushing the drift towards the target-present boundary) explained the neutral bias
286 observed with SDT criterion (c around zero for liberal, see Figure 2C).

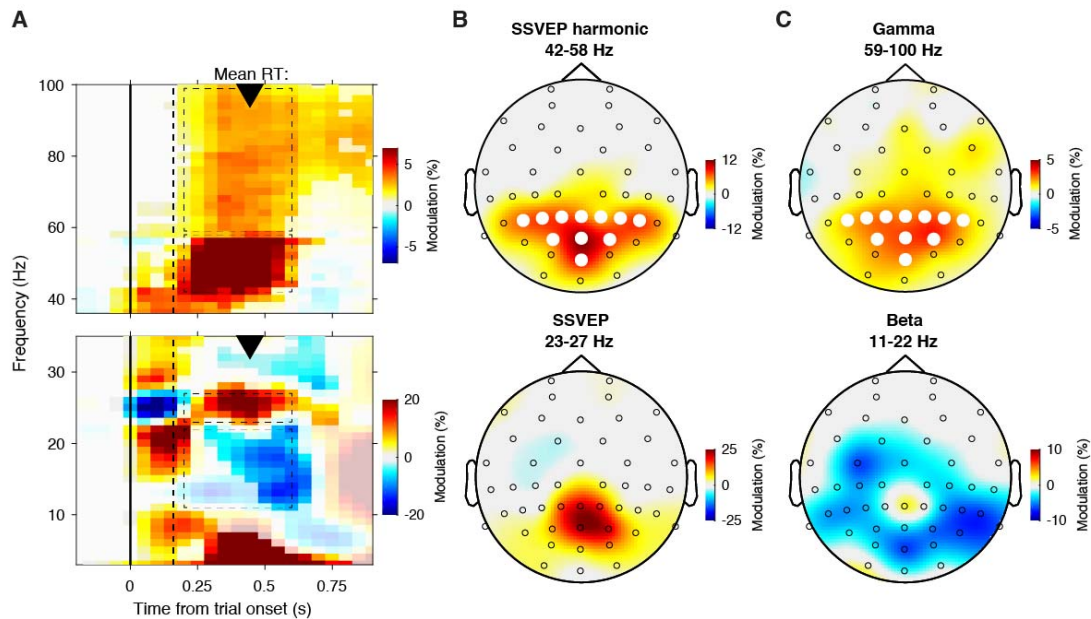
287 Convergent with these modelling results, drift bias was strongly anti-correlated
288 across participants with both SDT criterion (liberal, $r = -0.83$; conservative, $r = -0.79$)
289 and reaction times (liberal, $r = -0.66$; conservative, $r = -0.76$, all p -values < 0.005 ,
290 see Figure 2—figure supplement 2B and 2C). The strong correlations between drift
291 rate and d' on the one hand, and drift bias and c on the other, provide converging
292 evidence that the SDT and DDM frameworks capture similar underlying
293 mechanisms, while the DDM additionally captures the dynamic nature of perceptual
294 decision making by linking the decision bias manipulation to the evidence
295 accumulation process itself.

296 Finally, the bias manipulation also affected two other parameters in the drift
297 bias model that were not directly related to sensory evidence accumulation:
298 boundary separation was slightly but reliably higher during the liberal compared to
299 the conservative condition ($p < 0.0001$), and non-decision time (comprising time
300 needed for sensory encoding and motor response execution) was shorter during
301 liberal ($p < 0.0001$) (Figure 2—figure supplement 2D). In conclusion, a drift diffusion
302 model of choice behavior implementing a bias in sensory evidence accumulation
303 best explained how participants adjusted to the decision bias manipulations. In the
304 next sections, we used spectral analysis of the concurrent EEG recordings to identify
305 a plausible neural mechanism that implements biased sensory evidence
306 accumulation.

307

308 **Task-relevant textures induce stimulus-related responses in visual cortex**

309 Sensory evidence accumulation in a visual target detection task presumably relies
310 on stimulus-induced signals processed in visual cortex. Such stimulus-induced
311 signals are typically reflected in cortical population activity exhibiting a rhythmic
312 temporal structure (Buzsáki & Draguhn, 2004). Specifically, bottom-up processing of
313 visual information has previously been linked to increased high-frequency (> 40 Hz,
314 i.e. gamma) electrophysiological activity over visual cortex (Bastos et al., 2015;
315 Michalareas et al., 2016; Popov et al., 2017; van Kerkoerle et al., 2014). Figure 3A
316 shows time-frequency representations of EEG power modulations over posterior
317 cortex for the low- and high-frequency bands, normalized with respect to the
318 condition-specific pre-stimulus baseline period. We observed a total of four distinct
319 stimulus-induced power modulations after trial onset: two in the high-frequency
320 range (> 36 Hz, Figure 3A, top panel) and two in the low-frequency range (< 36 Hz,
321 Figure 3A, bottom panel). First, we found a spatially focal modulation in a narrow
322 frequency range around 25 Hz reflecting the steady state visual evoked potential
323 (SSVEP) arising from entrainment by the visual stimulation frequency of our
324 experimental paradigm (Figure 3B, lower panel). A second modulation from 42—58
325 Hz (Figure 3B, top panel) comprised the first harmonic of the SSVEP, as can be
326 seen from their similar topographic distributions (Figure 3B, compare top and lower
327 panel).



328

329 **Figure 3 | Task-relevant textures induce stimulus-induced responses in visual cortex.** A. Time-
330 frequency representations of high- (top) and low-frequency (bottom) EEG power modulations with
331 respect to the condition-specific pre-stimulus period (–0.4 to 0 s). Saturated colors indicate clusters of
332 significant modulation, cluster threshold $p < 0.05$, two-sided permutation test across participants,
333 cluster- \square corrected; $N = 15$). Solid and dotted vertical lines respectively indicate the onset of the trial
334 and the target stimulus. B. Scalp maps showing topography of the steady-state visual evoked
335 potential (SSVEP) power modulation around 25 Hz (bottom) and its harmonic from 42 – 58 Hz (top),
336 \square from 0.2 – 0.6 s after trial onset. C. 59 – 100 Hz gamma power modulation from 0.2 – 0.6 s (top)
337 and concurrent low frequency ('beta') power suppression from 11 – 22 Hz (bottom); see dashed
338 outlines \square on time-frequency representations in A. White dots indicate electrodes used for the time-
339 frequency representations in A, and which were selected for further analysis.

340 The following source data is available for Figure 3:

341 **Source data 1.** MATLAB .mat file containing the data used in panel A.

342 **Figure 3 – Figure supplement 1.** Liberal – conservative EEG power modulation contrast across
343 space, time and frequency.

344

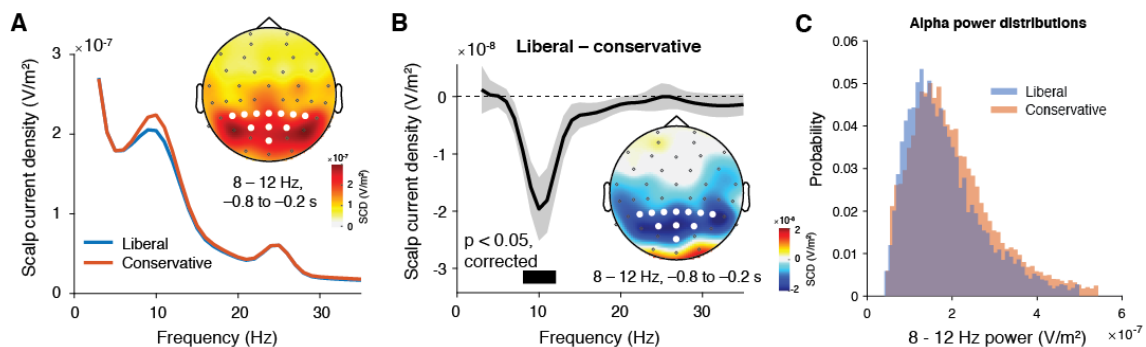
345 Third, we observed a 59—100 Hz gamma power modulation (Figure 3C, top
346 panel), after carefully controlling for high-frequency EEG artifacts due to small
347 fixational eye movements (microsaccades) by removing microsaccade-related
348 activity from the data (Hassler, Trujillo-Barreto, & Gruber, 2011; Hipp & Siegel, 2013;
349 Yuval-Greenberg, Tomer, Keren, Nelken, & Deouell, 2008), and by suppressing non-
350 neural EEG activity through scalp current density (SCD) transformation (Melloni,
351 Schwiedrzik, Wibral, Rodriguez, & Singer, 2009; Perrin, Pernier, Bertrand, &
352 Echallier, 1989) (see Methods for details). Importantly, the topography of the
353 observed gamma modulation was confined to posterior electrodes (electrodes
354 highlighted in Figures 3B and 3C, top panels), in line with the role of gamma in
355 bottom-up processing in visual cortex (Ni et al., 2016). Finally, we observed
356 suppression of low-frequency beta (11—22 Hz) activity in posterior cortex, which
357 typically occurs in parallel with enhanced stimulus-induced gamma activity (Donner
358 & Siegel, 2011; Kloosterman et al., 2015; Meindertsma, Kloosterman, Nolte, Engel,
359 & Donner, 2017; Werkle-Bergner et al., 2014)(Figure 3A and 3C, lower panels).
360 Taken together, we observed several different stimulus-induced power modulations
361 in posterior cortex. In the next section, we used the topographies of the high-
362 frequency poststimulus effects in visual cortex (Figures 3B and 3C, top panels) to
363 identify a pre-stimulus neural mechanism that could explain the observed biased
364 evidence accumulation resulting from the experimental decision bias manipulation.

365

366 **Adopting a liberal decision bias suppresses pre-stimulus alpha power**

367 Next, we tested whether our bias manipulation affected the amplitude of pre-stimulus
368 8—12 Hz (alpha) oscillations in visual cortex. To this end, we examined the raw, low-
369 frequency spectral power in the pre-stimulus interval in which a link between

370 spontaneous alpha fluctuations and decision bias has previously been reported (0.8
371 to 0.2 s before trial onset) (Iemi et al., 2017). We focused this analysis on cortical
372 regions processing visual information by selecting the electrode pooling that showed
373 stimulus-induced high-frequency gamma power modulation (see Figures 3B and
374 3C). Spectral power averaged across the two conditions indeed uncovered a highly
375 specific modulation around 10 Hz, which we confirmed to be strongest in the same
376 electrodes that showed strong modulation in the gamma range (Figure 4A, white
377 dots indicate electrodes showing stimulus-induced gamma modulation). Crucially,
378 the liberal – conservative difference between conditions revealed a statistically
379 significant cluster of suppressed frequencies precisely in the 8–12 Hz frequency
380 range ($p < 0.05$, cluster-corrected for multiple comparisons), which again showed a
381 posterior topography (Figure 4B). This small but highly consistent shift in the range in
382 which alpha occurs during the liberal compared to the conservative condition is
383 depicted in Figure 4C. Taken together, these findings show that a strategic liberal
384 bias shift suppresses pre-stimulus alpha power, suggesting that alpha modulations
385 are a hallmark of strategic bias adjustment rather than a mere correlate of
386 spontaneous shifts in decision bias. Importantly, this finding implies that humans are
387 able to actively control pre-stimulus alpha power in visual cortex, plausibly acting to
388 bias sensory evidence accumulation towards the response alternative that
389 maximizes rewards.



390

391 **Figure 4 | Adopting a liberal decision bias suppresses pre-stimulus alpha power. A.** Low-
392 frequency raw power spectra of pre-stimulus neural activity for both conditions based on the
393 electrodes that show large poststimulus power modulations in Figures 3B and 3C (top panels). Inset,
394 scalp map of raw pre-stimulus EEG alpha power (8 — 12 Hz neural activity between 0.8 and 0.2 s
395 before trial onset), pooled over conditions. White symbols indicate visual cortical electrodes used for
396 the raw power spectra in A. and B. **B.** Liberal – conservative raw power spectrum. Black horizontal
397 bar indicates statistically significant frequency range ($p < 0.05$, cluster-corrected for multiple
398 comparisons, two-sided). Error bars, SEM across participants ($N = 15$). Inset, corresponding liberal –
399 conservative scalp map of the pre-stimulus raw power difference between conditions. SCD, scalp
400 current density. **C.** Probability density distributions of single trial alpha power values for both
401 conditions, averaged across participants.

402 The following source data is available for Figure 4:

403 **Source data 1.** MATLAB .mat file containing the data used in panel B.

404

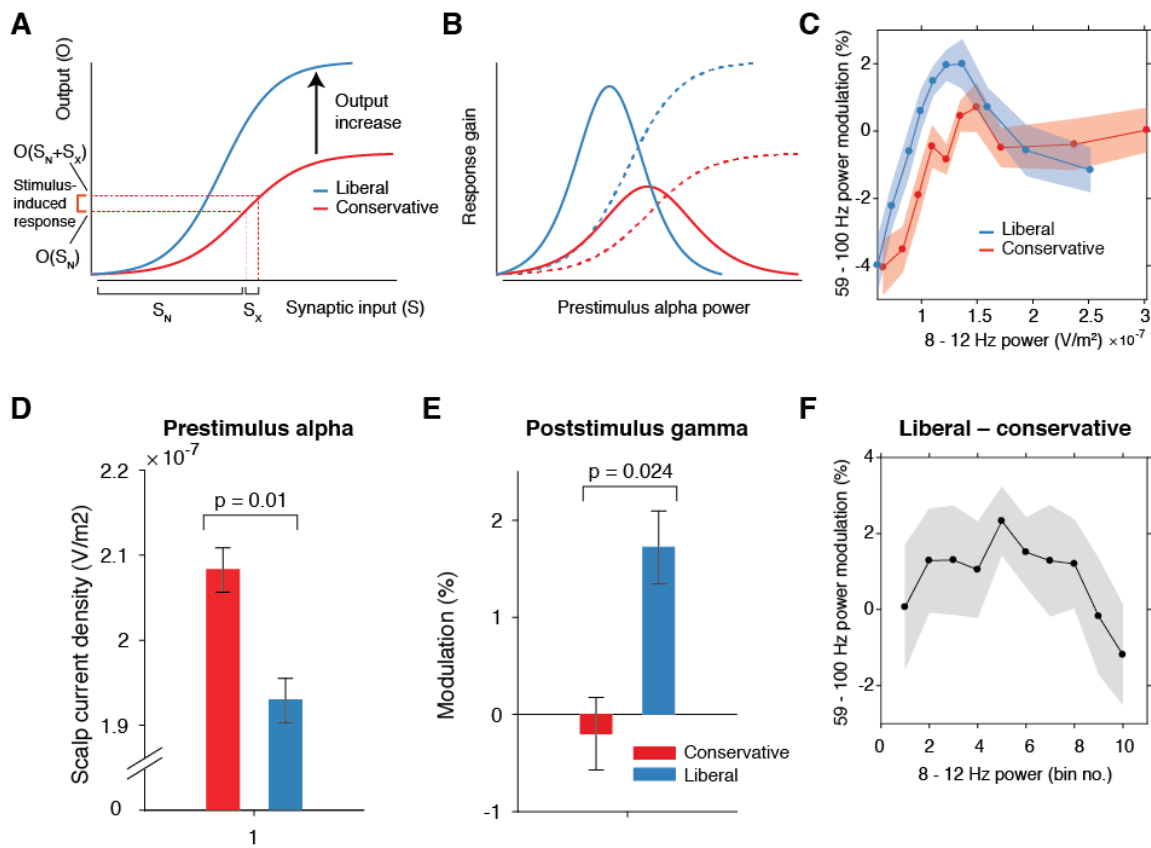
405 **Pre-stimulus alpha power mediates cortical gamma responses**

406 How could suppression of pre-stimulus alpha activity bias the process of sensory
407 evidence accumulation? One possibility is that alpha suppression influences
408 evidence accumulation by modulating the susceptibility of visual cortex to sensory
409 stimulation, a phenomenon dubbed ‘neural excitability’ (Iemi et al., 2017; Jensen &
410 Mazaheri, 2010). We explored this possibility using a theoretical response gain
411 model coined by Rajagovindan and Ding (2011). This model postulates that the
412 relationship between the total synaptic input activity that a neuronal ensemble
413 receives and the total output activity it produces is characterized by a sigmoidal
414 function (red line in Figure 5A) – a notion that is biologically plausible (Destexhe,
415 Rudolph, Fellous, & Sejnowski, 2001; Freeman, 1979). In this model, sensory input
416 (i.e. due to sensory stimulation) and ongoing fluctuations in endogenously generated
417 (i.e. not sensory-related) neural activity together comprise the synaptic input into

418 visual cortex. In our experiment, the sensory input into visual cortex can be assumed
419 to be identical across trials, because the same sensory stimulus was presented in
420 each trial (see Figure 2A). The endogenous input, in contrast, varies from trial to trial
421 reflecting fluctuations in top-down cognitive processes such as attention, and is
422 assumed to be reflected in alpha power. Given the combined constant sensory and
423 variable endogenous input in each trial (see horizontal axis in Figure 5A), the
424 strength of the output responses of visual cortex are largely determined by the trial-
425 to-trial variation caused by endogenous activity (see vertical axis in Figure 5A).
426 Furthermore, the sigmoidal shape of the input-output function results in an effective
427 range in the center of the function's input side which yields the strongest stimulus-
428 induced output responses since the sigmoid curve there is steepest. Mathematically,
429 the effect of endogenous input on stimulus-induced output responses (see marked
430 interval in Figure 5A) can be expressed as the first order derivative or slope of the
431 sigmoid in Figure 5A, which is referred to as the response gain by Rajagovindan and
432 Ding (2011). This derivative is plotted in Figure 5B (red line) across levels of pre-
433 stimulus alpha power, predicting an inverted-U shaped relationship between alpha
434 and response gain in visual cortex.

435 Regarding our experimental conditions, the model not only predicts that the
436 suppression of pre-stimulus alpha observed in the liberal condition reflects a shift in
437 the operational range of alpha (see Figure 4C), but also that it increases the
438 maximum output of visual cortex (a shift from the red to the blue line in figure 5A).
439 Thus, as the operational range of alpha shifts leftwards from conservative to liberal,
440 the upper asymptote in Figure 5A moves upwards such that the total maximum
441 output activity increases. This in turn affects the inverted-U-shaped relationship

442 between alpha and gain in visual cortex (blue line in Figure 5B), leading to a steeper
 443 response curve in the liberal condition resembling a Gaussian (bell-shaped) function.



444

445 **Figure 5 | Pre-stimulus alpha power mediates cortical gamma responses.** **A.** Theoretical
 446 response gain model describing the transformation of stimulus-induced and endogenous input activity
 447 (denoted by S_x and S_N respectively) to the total output activity (denoted by $O(S_x + S_N)$) in visual cortex
 448 by a sigmoidal function. Different operational alpha ranges are associated with input-output functions
 449 with different slopes due to corresponding changes in the total output. **B.** Alpha-mediated output
 450 responses (solid lines) are formalized as the first derivative (slope) of the sigmoidal functions (dotted
 451 lines), resulting in inverted-U (Gaussian) shaped relationships between alpha and gamma, involving
 452 stronger response gain in the liberal than in the conservative condition **C.** Corresponding empirical
 453 data showing gamma modulation (same percent signal change units as in Figure 3) as a function of
 454 alpha bin. The location on the x-axis of each alpha bin was taken as the median alpha of the trials
 455 assigned to each bin and averaged across subjects. **D-F.** Model prediction tests. **D.** Raw pre-stimulus
 456 alpha power for both conditions, averaged across subjects. **E.** Post-stimulus gamma power

457 modulation for both conditions averaged across the two middle alpha bins (5 and 6) in panel C. **F.**
458 Liberal – conservative difference between the response gain curves shown in panel C, centered on
459 alpha bin. Error bars, within-subject SEM across participants (N = 14).

460

461 The following source data is available for Figure 5:

462 **Source data 1.** SPSS .sav file containing the data used in panels C, E, and F.

463

464 To investigate sensory response gain across different alpha levels in our data,
465 we used the post-stimulus gamma activity (see Figure 3) as a proxy for alpha-
466 mediated output gain in visual cortex (Bastos et al., 2015; Michalareas et al., 2016;
467 Ni et al., 2016; Popov et al., 2017; van Kerkoerle et al., 2014). We exploited the large
468 number of trials per participant per condition (range 543 to 1391 trials) by sorting
469 each participant's trials into ten equal-sized bins ranging from weak to strong alpha,
470 separately for the two conditions. We then calculated the average gamma power
471 modulation within each alpha bin and finally plotted the participant-averaged gamma
472 across alpha bins in Figure 5C (see Methods for details). This indeed revealed an
473 inverted-U shaped relationship between alpha and gamma, with a steeper curve for
474 the liberal condition.

475 To assess the model's ability to explain the data, we statistically tested three
476 predictions derived from the model. First, the model predicts overall lower average
477 pre-stimulus alpha power for liberal than for conservative due to the shift in the
478 operational range of alpha. This was confirmed in Figure 5D ($p = 0.01$, permutation
479 test, see also Figures 4B and 4C). Second, the model predicts a stronger gamma
480 response for liberal than for conservative around the peak of the gain curve (the
481 center of the effective alpha range, see Figure 5B), which we indeed observed ($p =$
482 0.024 , permutation test on the average of the middle two alpha bins)(Figure 5E).

483 Finally, the model predicts that the difference between the gain curves (when they
484 are aligned over their effective ranges on the x-axis using alpha bin number, as
485 shown in Figure 5 – figure supplement 1A, also resembles a Gaussian curve (Figure
486 5 – figure supplement 1B). Consistent with this prediction, we observed an
487 interaction effect between condition (liberal, conservative) and bin number (1-10)
488 using a standard Gaussian contrast in a 2-way repeated measures ANOVA ($F(1,13)$
489 $= 4.6$, $p = 0.051$, partial $\eta^2 = 0.26$). Figure 5F illustrates this finding by showing the
490 difference between the two curves in Figure 5C as a function of alpha bin number
491 (see Figure 5 – figure supplement 1C for the curves of both conditions as a function
492 of alpha bin number). Subsequent separate tests for each condition indeed
493 confirmed a significant U-shaped relationship between alpha and gamma in the
494 liberal condition with a large effect size ($F(1,13) = 7.7$, $p = 0.016$, partial $\eta^2 = 0.37$),
495 but no significant effect in the conservative condition with only a small effect size
496 ($F(1,13) = 1.7$, $p = 0.22$, partial $\eta^2 = 0.12$, one-way repeated measures ANOVA's
497 with factor alpha bin, Gaussian contrast).

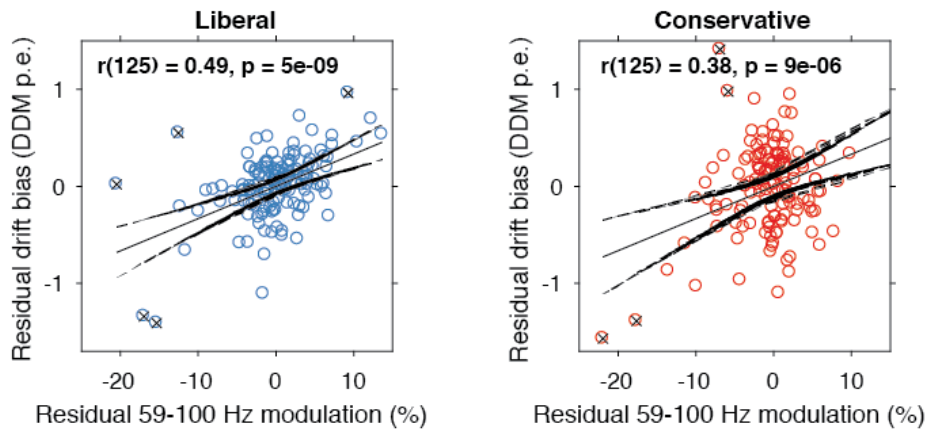
498 Taken together, these findings suggest that the alpha suppression observed
499 in the liberal compared to the conservative condition boosted stimulus-induced
500 activity in the liberal condition, which in turn might have indiscriminately biased
501 sensory evidence accumulation towards the target-present decision boundary. In the
502 next section, we investigate a direct link between drift bias and stimulus-induced
503 activity as measured through gamma.

504

505 **Visual cortical gamma activity predicts strength of evidence accumulation bias**

506 The findings presented so far suggest that behaviorally, a liberal decision bias shifts
507 evidence accumulation towards target-present responses (drift bias in the DDM),
508 while neurally it suppresses pre-stimulus alpha while enhancing poststimulus gamma
509 responses. In a final analysis, we asked whether alpha-binned gamma modulation is
510 directly related to a stronger drift bias. To this end, we again applied the drift bias
511 DDM to the behavioral data of each participant, but now freed the drift bias
512 parameter not only for the two conditions, but also for the ten alpha bins for which we
513 calculated gamma modulation (see Figure 5C). We directly tested the
514 correspondence between DDM drift bias and gamma modulation using repeated
515 measures correlation (Bakdash and Marusich, (2017), which takes all repeated
516 observations across participants into account while controlling for non-independence
517 of observations collected within each participant (see Methods for details). Gamma
518 modulation was indeed correlated with drift bias in both conditions (liberal, $r(125) =$
519 0.49 , $p = 5e-09$; conservative, $r(125) = 0.38$, $p = 9e-06$). We tested the robustness of
520 these correlations by excluding the data points that contributed most to the
521 correlations (as determined with Cook's distance) and obtained qualitatively similar
522 results, indicating these correlations were not driven by outliers (Figure 6, see
523 Methods for details). As a final control, we also performed this analysis for the
524 SSVEP (23-27 Hz) power modulation (see Figure 3B, bottom) and found a similar
525 inverted-U shaped relationship between alpha and the SSVEP for both conditions
526 (Figure 6 – figure supplement 1A), but no correlation with drift bias (Figure 6 – figure
527 supplement 1B). This suggests that the SSVEP is similarly coupled to alpha as the
528 stimulus-induced gamma, but is unaffected by the experimental conditions and not
529 predictive of decision bias shifts. Taken together, these results suggest that gamma
530 modulation underlies biased sensory evidence accumulation.

531



532

533 **Figure 6 | Alpha-binned gamma modulation correlates with evidence accumulation bias.**

534 Repeated measure correlation between gamma modulation and drift bias for the two conditions. Each
535 circle represents a participant's gamma modulation within one alpha bin. Drift bias and gamma
536 modulation scalars were residualized by removing the average within each participant and condition,
537 thereby removing the specific range in which the participants values operated. Crosses indicate data
538 points that were most influential for the correlation, identified using Cook's distance. Correlations
539 remained qualitatively unchanged when these data points were excluded (liberal, $r(120) = 0.43$, $p =$
540 $8e-07$; conservative, $r(121) = 0.32$, $p = 0.0003$) Error bars, 95% confidence intervals after averaging
541 across participants.

542 The following source data and figure supplements are available for Figure 6:

543 **Source data 1.** MATLAB .mat file containing the data used.

544 **Figure supplement 1.** Alpha-binned post-stimulus SSVEP modulation.

545

546 Discussion

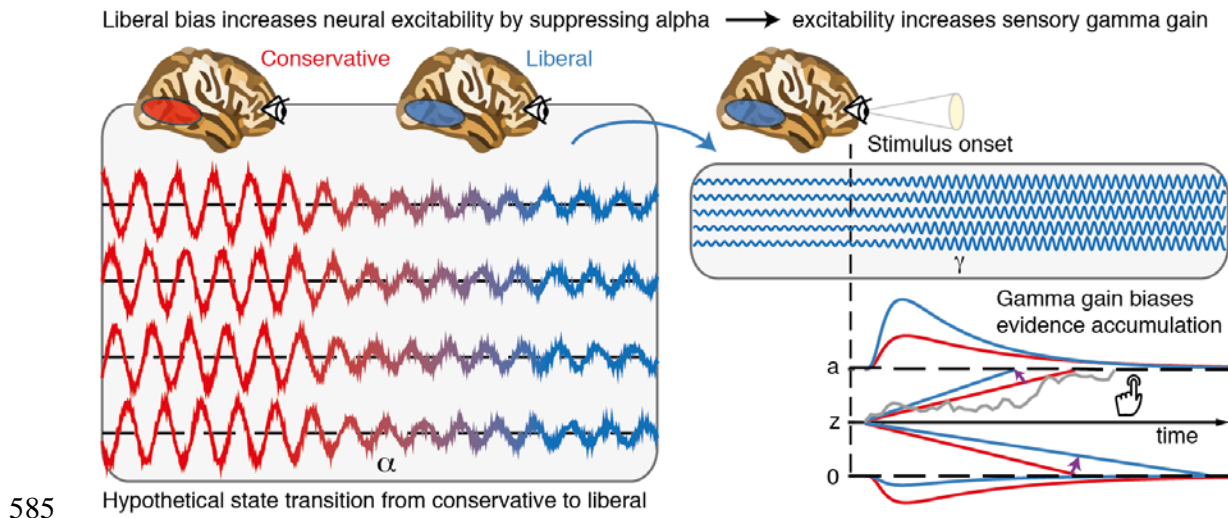
547 Traditionally, bias has been conceptualized in SDT as a criterion threshold that is
548 positioned at an arbitrary location between noise and signal-embedded-in-noise
549 distributions of sensory evidence strengths. The ability to strategically shift decision
550 bias in order to flexibly adapt to stimulus-response reward contingencies in the
551 environment presumably increases chances of survival, but to date such strategic

552 bias shifts as well as their neural underpinnings have not been demonstrated. Here,
553 we used a DDM drift bias model to show that an experimentally induced bias shift
554 affects the process of sensory evidence accumulation itself, rather than shifting a
555 threshold entity as SDT implies. Moreover, we reveal the neural signature of drift
556 bias by showing that a liberal decision bias increases alpha suppression (neural
557 excitability) of visual cortex, and enhancing gamma activity by increasing response
558 gain.

559 Although previous studies have shown correlations between suppression of
560 pre-stimulus alpha (8—12 Hz) power and a liberal decision bias during spontaneous
561 fluctuations in alpha activity (Iemi et al., 2017; Limbach & Corballis, 2016), these
562 studies have not established the effect of experimentally induced bias shifts within
563 person. In the current study, by experimentally manipulating stimulus-response
564 reward contingencies we show for the first time that pre-stimulus alpha can be
565 actively modulated by a participant to achieve changes in decision bias. Further, we
566 show that alpha suppression in turn modulates gamma activity, in part by increasing
567 the gain of cortical responses. Critically, gamma activity accurately predicted the
568 strength of the drift bias parameter in the DDM drift bias model, thereby linking our
569 behavioral and neural findings directly. Together, these findings show for the first
570 time that humans are able to actively implement decision biases by flexibly adapting
571 neural excitability to strategically shift sensory evidence accumulation towards one of
572 two decision bounds.

573 Based on our results, we propose that decision biases are implemented by
574 flexibly adjusting neural excitability in visual cortex. Figure 7 summarizes this
575 proposed mechanism graphically by visualizing a hypothetical transition in neural
576 excitability following a strategic liberal bias shift, as reflected in visual cortical alpha

577 suppression (left panel). This increased excitability translates into stronger gamma-
578 band responses following stimulus onset (right panel, top). These increased gamma
579 responses finally bias evidence accumulation towards the target-present decision
580 boundary during a liberal state, resulting in more target-present responses, whereas
581 target-absent responses are decimated (blue RT distributions; right panel, bottom).
582 Our experimental manipulation of decision bias in different blocks of trials suggests
583 that decision makers are able to control this biased evidence accumulation
584 mechanism willfully by adjusting excitability, as reflected in alpha.



586 **Figure 7 | Illustrative graphical depiction of the excitability state transition from conservative**
587 **to liberal, and subsequent biased evidence accumulation under a liberal bias.** The left panel
588 shows the transition from a conservative to a liberal condition block. The experimental induction of a
589 liberal decision bias causes alpha suppression in visual cortex, which increases neural excitability.
590 The right top panel shows increased gamma gain for incoming sensory evidence under conditions of
591 high excitability. The right bottom panel shows how increased gamma-gain causes a bias in the drift
592 rate, resulting in more 'target present' responses than in the conservative state.

593

594 A neural mechanism that could underlie bias-related alpha suppression may
595 be under control of the catecholaminergic neuromodulatory systems, consisting of

596 the noradrenaline-releasing locus coeruleus (LC) and dopamine systems (Aston-
597 Jones & Cohen, 2005). These systems are able to modulate the level of arousal and
598 neural gain, and show tight links with pupil responses (de Gee et al., 2017; de Gee,
599 Knapen, & Donner, 2014; Joshi, Li, Kalwani, & Gold, 2015; McGinley, David, &
600 McCormick, 2015). Accordingly, pre-stimulus alpha power suppression has also
601 recently been linked to pupil dilation (Meindertsma et al., 2017). From this
602 perspective, our results reconcile previous studies showing relationships between a
603 liberal bias, suppression of spontaneous alpha power and increased pupil size.
604 Consistent with this, a recent monkey study observed increased neural activity
605 during a liberal bias in the superior colliculus (Crapse, Lau, & Basso, 2018), a mid-
606 brain structure tightly interconnected with the LC (Joshi et al., 2015). Taken together,
607 a more liberal within-person bias (following experimental instruction and/or reward)
608 might activate neuromodulatory systems that subsequently increase cortical
609 excitability and enhance sensory responses for both stimulus and 'noise' signals in
610 visual cortex, thereby increasing a person's propensity for target-present responses
611 (Iemi et al., 2017).

612 We note that although the gain model is consistent with our data as well as
613 the data on which the model was conceived (see Rajagovindan & Ding, 2011), we do
614 not provide a plausible mechanism that could bring about the steepening in the U-
615 curved function observed in Figures 5C and 5F. Although Rajagovindan and Ding
616 report a simulation in their paper suggesting that increased excitability could indeed
617 cause increased gain, this shift could in principle either be caused by the alpha
618 suppression itself, by the same signal that causes alpha suppression, or it could
619 originate from an additional top-down signal from frontal brain regions. To investigate
620 this latter possibility, we performed a control analysis contrasting the conditions

621 simultaneously across space, time and frequency to test whether any frontal brain
622 region shows differences between conditions (see Figure 3 – figure supplement 1).
623 We did not find any such regions, even when using a less stringent test by omitting
624 the required correction for multiple comparisons. Thus, how exactly the gain
625 enhancement comes about remains an open question that should be addressed in
626 future research.

627 Whereas we report a unique link between alpha-mediated gamma modulation
628 and decision bias through the gain model, several previous studies have reported a
629 link between alpha and objective performance instead of bias, particularly in the
630 phase of alpha oscillations (Busch, Dubois, & VanRullen, 2009; Mathewson, Gratton,
631 Fabiani, Beck, & Ro, 2009). Our findings can be reconciled with those by considering
632 that detection sensitivity in many previous studies was often quantified in terms of
633 raw stimulus detection rates, which do not dissociate objective sensitivity from
634 response bias (see Figure 2B) (Green & Swets, 1966). Indeed, our findings are in
635 line with recently reported links between decision bias and spontaneous fluctuations
636 in excitability (Iemi et al., 2017; Iemi & Busch, 2017; Limbach & Corballis, 2016),
637 suggesting an active role of neural excitability in decision bias.

638 Further, one could ask whether the observed change in cortical excitability
639 may reflect a change in target detection sensitivity (drift rate) rather than an
640 intentional bias shift. This is unlikely because that would predict effects opposite to
641 those we observed. We found increased excitability in the liberal condition compared
642 to the conservative condition; if this were related to improved detection performance,
643 one would predict higher sensitivity in the liberal condition, while we rather found
644 higher sensitivity in the conservative condition (compare drift rate to drift bias in both
645 conditions in Fig. 2C). This finding convincingly ties cortical excitability in our

646 paradigm to decision bias, as opposed to detection sensitivity. Convergently, other
647 studies also report a link between pre-stimulus low-frequency EEG activity and
648 subjective perception, but not objective task performance (Benwell et al., 2017; Iemi
649 & Busch, 2017).

650 In summary, our results suggest that stimulus-induced responses are boosted
651 during a liberal decision bias due to increased cortical excitability, in line with recent
652 work linking alpha power suppression to response gain (Peterson & Voytek, 2017).
653 Future studies can now establish whether this same mechanism is at play in other
654 subjective aspects of decision-making, such as confidence and meta-cognition
655 (Fleming, Putten, & Daw, 2018; Samaha et al., 2017) as well as in a dynamically
656 changing environment (Norton, Fleming, Daw, & Landy, 2017). Explicit manipulation
657 of cortical response gain during a bias manipulation (by pharmacological
658 manipulation of the noradrenergic LC-NE system; (Servan-Schreiber, Printz, &
659 Cohen, 1990)) or by enhancing occipital alpha power using transcranial brain
660 stimulation (Zaehle, Rach, & Herrmann, 2010) could further establish the underlying
661 neural mechanisms involved in decision bias.

662 In the end, although one may be unaware, every decision we make is
663 influenced by biases that operate on one's noisy evidence accumulation process.
664 Understanding how these biases affect our decisions is crucial to enable us to
665 control or invoke them adaptively (Pleskac, Cesario, & Johnson, 2017). Pinpointing
666 the neural mechanisms underlying bias in the current elementary perceptual task
667 may pave the way for understanding how more abstract and high-level decisions are
668 modulated by decision bias (Tversky & Kahneman, 1974).

669

670 **Acknowledgments**

671 The authors thank Timothy J. Pleskac for discussion.

672

673 **Declaration of Interests**

674 The authors declare no competing interests.

675

676 **Data and code sharing**

677 The data analyzed in this study are publicly available on Figshare (Kloosterman et
678 al., 2018). Analysis scripts are publicly available on Github
679 (<https://github.com/nkloost1/critEEG>).

680

681 **Source data and figure supplements**

682 The following source data and figure supplements are included in this article:

683 Figure 2 – Figure supplements 1, 2 and 3.

684 Figure 2 – Source data 1. (source_Figure2.csv)

685 Figure 3 – Source data 1. (source_Figure3.mat.zip)

686 Figure 3 – Figure supplement 1

687 Figure 4 – Source data 1. (source_Figure4.mat.zip)

688 Figure 5 – Source data 1. (source_Figure5.sav.zip)

689 Figure 6 – Source data 1. (source_Figure6.mat.zip)

690 Figure 6 – Figure supplement 1.

691

692 **Figure supplement legends**

693 **Figure 2—figure supplement 1** | Behavioral and neurophysiological evidence that participants were
694 sensitive to the implicit task structure. **A.** Participant-average RT distributions for hits and false alarms
695 in both conditions. The presence of similar RT distributions for false alarms and hits indicates that
696 participants were sensitive to trial onset despite the fact that trial onsets were only implicitly signaled.
697 Error bars, SEM. **B.** Time-frequency representations of low-frequency EEG power modulations with
698 respect to the pre-stimulus period (−0.4 – 0 s), pooled across the two conditions. Significant low-
699 frequency modulation occurred even for nontarget trials without overt response (correct rejections),
700 indicating that participants detected the onset of a trial even when neither a target was presented nor
701 a response was given. Saturated colors indicate clusters of significant modulation, cluster threshold p
702 < 0.05, two-sided permutation test across participants, cluster- \square corrected; $N = 15$). Solid and dotted
703 vertical lines respectively indicate the onset of the trial and the target stimulus. M, power modulation.

704

705 **Figure 2—figure supplement 2** | **Signal-detection-theoretic (SDT) behavioral measures during**
706 **both conditions correspond closely to drift diffusion modeling (DDM) parameters.** **A.** Across-
707 participant Pearson correlation between d' and drift rate for the two conditions. Each dot represents a
708 participant. **B.** As A. but for correlation between criterion and DDM drift bias. The correlation is
709 negative due to a lower criterion reflecting a stronger liberal bias. **C.** Left panel, mean reaction times
710 (RT) for hits and false alarms for the two conditions. Middle and right panels, As A. but for correlation
711 between RT for hits and drift bias. **D.** Parameter estimates in the drift bias DDM not related to
712 evidence accumulation (drift rate). *** $p < 0.001$; n.s., not significant.

713

714 **Figure 2—figure supplement 3** | **Single-participant drift diffusion model fits for the drift bias**
715 **model for both conditions.** Pink bars, number of implicit target-absent choices; Green bars, RT
716 distribution quantiles for target-present choices; dotted lines, model fits for the drift bias model.

717

718 **Figure 3 – figure supplement 1** | **Liberal – conservative contrast of EEG power modulations**
719 **across space, time and frequency.** The two conditions were contrasted across space-time-
720 frequency bins using paired t-tests performed at each bin. Single bins were subsequently thresholded
721 at $p < 0.05$ and clusters of contiguous bins were determined. Cluster significance was assessed using
722 a cluster-based permutation procedure (1000 permutations). For visualization purposes, we
723 integrated (using the matlab trapz function) power modulation in the time-frequency representations
724 (TFR's, left panels) across the highlighted electrodes in the topographies (right panels). For the
725 topographies, modulation was integrated across the saturated time-frequency bins in the TFR's.
726 Saturated colors indicate bins that are part of clusters. p -values above the topographies indicate

727 cluster significance level tested across participants; $N = 14$). **A.** We found one significant cluster of
728 positive sign ($p = 0.005$) located in the most occipital electrodes (I1, I2, and I3, extending towards
729 parietal regions) spanning the complete high-frequency range (> 20 Hz), reflecting enhanced broad-
730 band gamma activity in the liberal condition. Note that our selected electrode pooling (see Figure 2)
731 did not include these electrodes. **B.** Further, we observed one marginally significant negative cluster
732 ($p = 0.11$) comprising the pre-stimulus alpha-suppression in the liberal condition (as reported in the
733 manuscript) that was connected across time with alpha-beta band activity over motor cortex around
734 the time of report (~ -0.5 s). Note that all participants responded with their right hand, yielding stronger
735 left-lateralized motor-related activity. **C.** Finally, we observed a transient positive cluster around 10 Hz
736 from 0.4 s post-trial onset with a spatial topography similar to the cluster in A, which was not
737 significant ($p = 0.35$). This cluster possibly reflects either a stronger event-related potential, or
738 stronger transient enhancement of theta oscillations (4–8 Hz) in the liberal condition around the time
739 of the response. Topographies in all panels appear quite similar due to the strong modulation of the
740 cluster depicted in panel A. However, the cortical locations of clusters in each panel are indicated by
741 the thick black dots that indicate electrodes that are part of the cluster. Taken together, we observe no
742 strong evidence for a frontal cluster that could potentially underlie the steepened inverse-U shape
743 during the liberal condition observed in visual cortex.

744

745 **Figure 5 – figure supplement 1 | Gain model predictions and corresponding empirical data**
746 **plotted as a function of pre-stimulus alpha bin number. A.** Model predictions for both conditions.
747 The gain curve for the liberal condition is steeper than for the conservative condition. Binning trials
748 based on alpha within each condition directly maps the peaks of the gain curves onto each other. **B.**
749 Model prediction for liberal – conservative as a function of alpha bin number. The difference gain
750 curve between the two conditions is again an inverted-U shaped function. **C.** Corresponding empirical
751 data. The plot is identical to Figure 5C, except that the bin number is plotted instead of the actual
752 alpha power for each condition.

753

754 **Figure 6 – figure supplement 1 | Alpha-binned post-stimulus SSVEP modulation. A.** Inverted-U
755 shaped relationship between alpha and SSVEP modulation, computed as the percent signal change
756 23 – 27 Hz power modulation with respect to the pre-stimulus baseline. **B.** Correlations between
757 SSVEP modulation and drift bias for both conditions. These non-significant correlations are overall
758 weaker than for gamma (see Figure 6).

759

760 **References**

- 761 Aston-Jones, G., & Cohen, J. D. (2005). An integrative theory of locus coeruleus-
762 norepinephrine function: adaptive gain and optimal performance. *Annual Review*
763 *of Neuroscience*, 28(1), 403–450.
764 <http://doi.org/10.1146/annurev.neuro.28.061604.135709>
765 Bakdash, J. Z., & Marusich, L. R. (2017). Repeated Measures Correlation. *Frontiers*
766 *in Psychology*, 8, 491. <http://doi.org/10.3389/fpsyg.2017.00456>

- 767 Bastos, A. M., Vezoli, J., Bosman, C. A., Schoffelen, J.-M., Oostenveld, R., Dowdall,
768 J. R., et al. (2015). Visual Areas Exert Feedforward and Feedback Influences
769 through Distinct Frequency Channels. *Neuron*, 85(2), 390–401.
770 <http://doi.org/10.1016/j.neuron.2014.12.018>
- 771 Benwell, C. S. Y., Tagliabue, C. F., Veniero, D., Cecere, R., Savazzi, S., & Thut, G.
772 (2017). Pre-stimulus EEG power predicts conscious awareness but not objective
773 visual performance. *eNeuro*, 4(6), ENEURO.0182–17.2017.
774 <http://doi.org/10.1523/ENEURO.0182-17.2017>
- 775 Bogacz, R., Brown, E., Moehlis, J., Holmes, P., & Cohen, J. D. (2006). The physics
776 of optimal decision making: A formal analysis of models of performance in two-
777 alternative forced-choice tasks. *Psychological Review*, 113(4), 700–765.
778 <http://doi.org/10.1037/0033-295X.113.4.700>
- 779 Busch, N. A., Dubois, J., & VanRullen, R. (2009). The Phase of Ongoing EEG
780 Oscillations Predicts Visual Perception. *Journal of Neuroscience*, 29(24), 7869–
781 7876. <http://doi.org/10.1523/JNEUROSCI.0113-09.2009>
- 782 Buzsáki, G., & Draguhn, A. (2004). Neuronal oscillations in cortical networks.
783 *Science (New York, NY)*, 304(5679), 1926–1929.
784 <http://doi.org/10.1126/science.1099745>
- 785 Crapse, T. B., Lau, H., & Basso, M. A. (2018). A Role for the Superior Colliculus in
786 Decision Criteria. *Neuron*, 97(1), 181–194.e6.
787 <http://doi.org/10.1016/j.neuron.2017.12.006>
- 788 de Gee, J. W., Colizoli, O., Kloosterman, N. A., Knapen, T., Nieuwenhuis, S., &
789 Donner, T. H. (2017). Dynamic modulation of decision biases by brainstem
790 arousal systems. *eLife*, 6, 309. <http://doi.org/10.7554/eLife.23232>
- 791 de Gee, J. W., Knapen, T., & Donner, T. H. (2014). Decision-related pupil dilation
792 reflects upcoming choice and individual bias. *Proceedings of the National
793 Academy of Sciences of the United States of America*, 111(5), E618–25.
794 <http://doi.org/10.1073/pnas.1317557111>
- 795 Destexhe, A., Rudolph, M., Fellous, J. M., & Sejnowski, T. J. (2001). Fluctuating
796 synaptic conductances recreate in vivo-like activity in neocortical neurons.
797 *Neuroscience*, 107(1), 13–24. [http://doi.org/10.1016/S0306-4522\(01\)00344-X](http://doi.org/10.1016/S0306-4522(01)00344-X)
- 798 Donner, T. H., & Siegel, M. (2011). A framework for local cortical oscillation patterns.
799 *Trends in Cognitive Sciences*, 15(5), 191–199.
800 <http://doi.org/10.1016/j.tics.2011.03.007>
- 801 Efron, B., & Tibshirani, R. (1998). The problem of regions. *The Annals of Statistics*,
802 26(5), 1687–1718. <http://doi.org/10.1214/aos/1024691353>
- 803 Fahrenfort, J. J., Scholte, H. S., & Lamme, V. A. F. (2007). Masking disrupts
804 reentrant processing in human visual cortex. *Journal of Cognitive Neuroscience*,
805 19(9), 1488–1497.
806 [http://doi.org/10.1162/jocn.2007.19.9.1488&url_ctx_fmt=info:ofi/fmt:kev:mtx:ctx&
807 ft_val_fmt=info:ofi/fmt:kev:mtx:journal&rft.atitle=Masking](http://doi.org/10.1162/jocn.2007.19.9.1488&url_ctx_fmt=info:ofi/fmt:kev:mtx:ctx&ft_val_fmt=info:ofi/fmt:kev:mtx:journal&rft.atitle=Masking)
- 808 Fahrenfort, J. J., Scholte, H. S., & Lamme, V. A. F. (2008). The spatiotemporal
809 profile of cortical processing leading up to visual perception. *Journal of Vision*,
810 8(1), 12–12. <http://doi.org/10.1167/8.1.12>
- 811 Fetsch, C. R., Kiani, R., & Shadlen, M. N. (2014). Predicting the Accuracy of a
812 Decision: A Neural Mechanism of Confidence. *Cold Spring Harbor Symposia on
813 Quantitative Biology*, 79, 185–197. <http://doi.org/10.1101/sqb.2014.79.024893>
- 814 Fleming, S. M., Putten, E. J., & Daw, N. D. (2018). Neural mediators of changes of
815 mind about perceptual decisions. *Nature Neuroscience*, 21(4), 617–624.
816 <http://doi.org/10.1038/s41593-018-0104-6>

- 817 Freeman, W. J. (1979). Nonlinear gain mediating cortical stimulus-response
818 relations. *Biological Cybernetics*, 33(4), 237–247.
819 <http://doi.org/10.1007/BF00337412>
- 820 Gold, J. I., & Shadlen, M. N. (2007). The neural basis of decision making. *Annual*
821 *Review of Neuroscience*, 30, 535–574.
822 <http://doi.org/10.1146/annurev.neuro.29.051605.113038>
- 823 Green, D. M., & Swets, J. A. (1966). Signal detection theory and psychophysics.
824 *Society*, 1, 521.
- 825 Hassler, U., Trujillo-Barreto, N., & Gruber, T. (2011). Induced gamma band
826 responses in human EEG after the control of miniature saccadic artifacts.
827 *NeuroImage*, 57(4), 1411–1421. <http://doi.org/10.1016/j.neuroimage.2011.05.062>
- 828 Hipp, J. F., & Siegel, M. (2013). Dissociating neuronal gamma-band activity from
829 cranial and ocular muscle activity in EEG. *Frontiers in Human Neuroscience*, 7,
830 338. <http://doi.org/10.3389/fnhum.2013.00338>
- 831 Iemi, L., & Busch, N. A. (2017). Moment-to-moment fluctuations in neuronal
832 excitability bias subjective perception rather than decision-making. *bioRxiv*,
833 151324. <http://doi.org/10.1101/151324>
- 834 Iemi, L., Chaumon, M., Crouzet, S. M., & Busch, N. A. (2017). Spontaneous Neural
835 Oscillations Bias Perception by Modulating Baseline Excitability. *The Journal of*
836 *Neuroscience : the Official Journal of the Society for Neuroscience*, 37(4), 807–
837 819. <http://doi.org/10.1523/JNEUROSCI.1432-16.2017>
- 838 Jensen, O., & Mazaheri, A. (2010). Shaping functional architecture by oscillatory
839 alpha activity: gating by inhibition. *Frontiers in Human Neuroscience*, 4, 186.
840 <http://doi.org/10.3389/fnhum.2010.00186>
- 841 Joshi, S., Li, Y., Kalwani, R. M., & Gold, J. I. (2015). Relationships between Pupil
842 Diameter and Neuronal Activity in the Locus Coeruleus, Colliculi, and Cingulate
843 Cortex. *Neuron*, 0(0), 221–234. <http://doi.org/10.1016/j.neuron.2015.11.028>
- 844 Kiani, R., Hanks, T. D., & Shadlen, M. N. (2008). Bounded Integration in Parietal
845 Cortex Underlies Decisions Even When Viewing Duration Is Dictated by the
846 Environment. *Journal of Neuroscience*, 28(12), 3017–3029.
847 <http://doi.org/10.1523/JNEUROSCI.4761-07.2008>
- 848 Kloosterman, N. A., de Gee, J. W., Werkle-Bergner, M., Lindenberger, U., Garrett, D.
849 D., & Fahrenfort, J. J. (2018). Data from: Humans strategically shift decision bias
850 by flexibly adjusting sensory evidence accumulation in visual cortex.
851 <http://doi.org/https://doi.org/10.6084/m9.figshare.6142940>
- 852 Kloosterman, N. A., Meindertsma, T., Hillebrand, A., van Dijk, B. W., Lamme, V. A.
853 F., & Donner, T. H. (2015). Top-down modulation in human visual cortex predicts
854 the stability of a perceptual illusion. *Journal of Neurophysiology*, 113(4), 1063–
855 1076. <http://doi.org/10.1152/jn.00338.2014>
- 856 Lamme, V. A. (1995). The neurophysiology of figure-ground segregation in primary
857 visual cortex. *Journal of Neuroscience*, 15(2), 1605–1615.
858 <http://doi.org/10.1523/JNEUROSCI.15-02-01605.1995>
- 859 Lamme, V. A. F., Zipser, K., & Spekreijse, H. (2006). Masking Interrupts Figure-
860 Ground Signals in V1. *Dx.Doi.org*, 14(7), 1044–1053.
861 <http://doi.org/10.1162/089892902320474490>
- 862 Limbach, K., & Corballis, P. M. (2016). Pre-stimulus alpha power influences
863 response criterion in a detection task. *Psychophysiology*, 53(8), 1154–1164.
864 <http://doi.org/10.1111/psyp.12666>

- 865 Maris, E., & Oostenveld, R. (2007). Nonparametric statistical testing of EEG-and
866 MEG-data. *Journal of Neuroscience Methods*, 164(1), 177–190.
867 <http://doi.org/10.1016/j.jneumeth.2007.03.024>
- 868 Mathewson, K. E., Gratton, G., Fabiani, M., Beck, D. M., & Ro, T. (2009). To See or
869 Not to See: Pre-stimulus α Phase Predicts Visual Awareness. *Journal of*
870 *Neuroscience*, 29(9), 2725–2732. [http://doi.org/10.1523/JNEUROSCI.3963-](http://doi.org/10.1523/JNEUROSCI.3963-08.2009)
871 08.2009
- 872 McGinley, M. J., David, S. V., & McCormick, D. A. (2015). Cortical Membrane
873 Potential Signature of Optimal States for Sensory Signal Detection. *Neuron*,
874 87(1), 179–192. <http://doi.org/10.1016/j.neuron.2015.05.038>
- 875 Meindertsma, T., Kloosterman, N. A., Nolte, G., Engel, A. K., & Donner, T. H. (2017).
876 Multiple Transient Signals in Human Visual Cortex Associated with an
877 Elementary Decision. *Journal of Neuroscience*, 37(23), 5744–5757.
878 <http://doi.org/10.1523/JNEUROSCI.3835-16.2017>
- 879 Melloni, L., Schwiedrzik, C. M., Wibrals, M., Rodriguez, E., & Singer, W. (2009).
880 Response to: Yuval-Greenberg et al., “Transient Induced Gamma-Band
881 Response in EEG as a Manifestation of Miniature Saccades.” *Neuron* 58, 429-
882 441. *Neuron*, 62(1), 8–10– author reply 10–12.
883 <http://doi.org/10.1016/j.neuron.2009.04.002>
- 884 Michalareas, G., Vezoli, J., van Pelt, S., Schoffelen, J.-M., Kennedy, H., & Fries, P.
885 (2016). Alpha-Beta and Gamma Rhythms Subserve Feedback and Feedforward
886 Influences among Human Visual Cortical Areas. *Neuron*, 89(2), 384–397.
887 <http://doi.org/10.1016/j.neuron.2015.12.018>
- 888 Mitra, P. P., & Pesaran, B. (1999). Analysis of Dynamic Brain Imaging Data.
889 *Biophysical Journal*, 76(2), 691–708. [http://doi.org/10.1016/S0006-](http://doi.org/10.1016/S0006-3495(99)77236-X)
890 3495(99)77236-X
- 891 Mulder, M. J., Wagenmakers, E.-J., Ratcliff, R., Boekel, W., & Forstmann, B. U.
892 (2012). Bias in the brain: a diffusion model analysis of prior probability and
893 potential payoff. *The Journal of Neuroscience : the Official Journal of the Society*
894 *for Neuroscience*, 32(7), 2335–2343. [http://doi.org/10.1523/JNEUROSCI.4156-](http://doi.org/10.1523/JNEUROSCI.4156-11.2012)
895 11.2012
- 896 Neath, A. A., & Cavanaugh, J. E. (2012). The Bayesian information criterion:
897 background, derivation, and applications. *Wiley Interdisciplinary Reviews:*
898 *Computational Statistics*, 4(2), 199–203. <http://doi.org/10.1002/wics.199>
- 899 Ni, J., Wunderle, T., Lewis, C. M., Desimone, R., Diester, I., & Fries, P. (2016).
900 Gamma-Rhythmic Gain Modulation. *Neuron*, 92(1), 240–251.
901 <http://doi.org/10.1016/j.neuron.2016.09.003>
- 902 Norton, E. H., Fleming, S. M., Daw, N. D., & Landy, M. S. (2017). Suboptimal
903 Criterion Learning in Static and Dynamic Environments. *PLoS Computational*
904 *Biology*, 13(1), e1005304–28. <http://doi.org/10.1371/journal.pcbi.1005304>
- 905 Oostenveld, R., Fries, P., Maris, E., & Schoffelen, J.-M. (2011). FieldTrip: open
906 source software for advanced analysis of MEG, EEG, and invasive
907 electrophysiological data. *Computational Intelligence and Neuroscience*, 2011(1),
908 1–9. <http://doi.org/10.1155/2011/156869>
- 909 Perrin, F., Pernier, J., Bertrand, O., & Echallier, J. F. (1989). Spherical splines for
910 scalp potential and current density mapping. *Electroencephalography and*
911 *Clinical Neurophysiology*, 72(2), 184–187. [http://doi.org/10.1016/0013-](http://doi.org/10.1016/0013-4694(89)90180-6)
912 4694(89)90180-6
- 913 Peterson, E. J., & Voytek, B. (2017). Alpha oscillations control cortical gain by
914 modulating excitatory-inhibitory background activity. *Biorxiv.org*

- 915 . <http://doi.org/https://doi.org/10.1101/185074>
- 916 Pleskac, T. J., Cesario, J., & Johnson, D. J. (2017). How race affects evidence
917 accumulation during the decision to shoot. *Psychonomic Bulletin & Review*,
918 18(2), 1–30. <http://doi.org/10.3758/s13423-017-1369-6>
- 919 Popov, T., Kastner, S., & Jensen, O. (2017). FEF-Controlled Alpha Delay Activity
920 Precedes Stimulus-Induced Gamma-Band Activity in Visual Cortex. *Journal of*
921 *Neuroscience*, 37(15), 4117–4127. [http://doi.org/10.1523/JNEUROSCI.3015-](http://doi.org/10.1523/JNEUROSCI.3015-2017)
922 16.2017
- 923 Rajagovindan, & Ding, M. (2011). From pre-stimulus alpha oscillation to visual-
924 evoked response: an inverted-U function and its attentional modulation. *Journal*
925 *of Cognitive Neuroscience*, 23(6), 1379–1394.
926 <http://doi.org/10.1162/jocn.2010.21478>
- 927 Ratcliff, R. (1978). A theory of memory retrieval. *Psychological Review*, 85(2), 59–
928 108. <http://doi.org/10.1037//0033-295X.85.2.59>
- 929 Ratcliff, R. (2006). Modeling response signal and response time data. *Cognitive*
930 *Psychology*, 53(3), 195–237. <http://doi.org/10.1016/j.cogpsych.2005.10.002>
- 931 Ratcliff, R., & McKoon, G. (2008). The Diffusion Decision Model: Theory and Data for
932 Two-Choice Decision Tasks. *Neural Computation*, 20(4), 873–922.
933 <http://doi.org/10.1162/neco.2008.12-06-420>
- 934 Ratcliff, R., Huang-Pollock, C., & McKoon, G. (2016, August 15). Modeling Individual
935 Differences in the Go/No-Go Task With a Diffusion Model. [http://doi.org/http://](http://doi.org/http://dx.doi.org/10.1037/dec0000065)
936 dx.doi.org/10.1037/dec0000065
- 937 Samaha, J., Lemi, L., & Postle, B. R. (2017). Pre-stimulus alpha-band power biases
938 visual discrimination confidence, but not accuracy. *Consciousness and*
939 *Cognition*. <http://doi.org/10.1016/j.concog.2017.02.005>
- 940 Servan-Schreiber, D., Printz, H., & Cohen, J. D. (1990). A network model of
941 catecholamine effects: gain, signal-to-noise ratio, and behavior. *Science (New*
942 *York, NY)*, 249(4971), 892–895.
- 943 Supèr, H., Spekreijse, H., letters, V. L. N., 2003. (2003). Figure–ground activity in
944 primary visual cortex (V1) of the monkey matches the speed of behavioral
945 response. *Elsevier*
946 , 344(2), 75–78. [http://doi.org/10.1016/S0304-3940\(03\)00360-4](http://doi.org/10.1016/S0304-3940(03)00360-4)
- 947 Tversky, A., & Kahneman, D. (1974). Judgment under Uncertainty: Heuristics and
948 Biases. *Science (New York, NY)*, 185(4157), 1124–1131.
949 <http://doi.org/10.1126/science.185.4157.1124>
- 950 Urai, A. E., de Gee, J. W., & Donner, T. H. (2018). Choice history biases subsequent
951 evidence accumulation. *bioRxiv*, 251595. <http://doi.org/10.1101/251595>
- 952 van Kerkoerle, T., Self, M. W., Dagnino, B., Gariel-Mathis, M.-A., Poort, J., van der
953 Togt, C., & Roelfsema, P. R. (2014). Alpha and gamma oscillations characterize
954 feedback and feedforward processing in monkey visual cortex. *Proceedings of*
955 *the National Academy of Sciences of the United States of America*, 111(40),
956 14332–14341. <http://doi.org/10.1073/pnas.1402773111>
- 957 Werkle-Bergner, M., Grandy, T. H., Chicherio, C., Schmiedek, F., Lovden, M., &
958 Lindenberger, U. (2014). Coordinated within-Trial Dynamics of Low-Frequency
959 Neural Rhythms Controls Evidence Accumulation. *Journal of Neuroscience*,
960 34(25), 8519–8528. <http://doi.org/10.1523/JNEUROSCI.3801-13.2014>
- 961 White, C. N., & Poldrack, R. A. (2014). Decomposing bias in different types of simple
962 decisions. *Journal of Experimental Psychology Learning, Memory, and*
963 *Cognition*, 40(2), 385–398. <http://doi.org/10.1037/a0034851>

- 964 Wiecki, T. V., Sofer, I., & Frank, M. J. (2013). HDDM: Hierarchical Bayesian
965 estimation of the Drift-Diffusion Model in Python. *Frontiers in Neuroinformatics*, 7.
966 <http://doi.org/10.3389/fninf.2013.00014>
967 Yuval-Greenberg, S., Tomer, O., Keren, A. S., Nelken, I., & Deouell, L. Y. (2008).
968 Transient Induced Gamma-Band Response in EEG as a Manifestation of
969 Miniature Saccades. *Neuron*, 58(3), 429–441.
970 <http://doi.org/10.1016/j.neuron.2008.03.027>
971 Zaehle, T., Rach, S., & Herrmann, C. S. (2010). Transcranial Alternating Current
972 Stimulation Enhances Individual Alpha Activity in Human EEG. *PLoS ONE*,
973 5(11), e13766. <http://doi.org/10.1371/journal.pone.0013766>
974
975

976 **Materials and Methods**

977 **Participants** Sixteen participants (eight females, mean age 24.1 years, \pm 1.64) took
978 part in the experiment, either for financial compensation (EUR 10, - per hour) or in
979 partial fulfillment of first year psychology course requirements. Each participant
980 completed three experimental sessions on different days, each session lasting ca. 2
981 hours, including preparation and breaks. One participant completed only two
982 sessions, yielding a total number of sessions across subjects of 47. Due to technical
983 issues, for one session only data for the liberal condition was available. One
984 participant was an author. All participants had normal or corrected-to-normal vision
985 and were right handed. Participants provided written informed consent before the
986 start of the experiment. All procedures were approved by the ethics committee of the
987 University of Amsterdam.

988 Regarding sample size, our experiment consisted of 16 biological replications
989 (participants) and either two (one participant) or three (fifteen participants) technical
990 replications (i.e. experimental sessions). The sample size was determined based on
991 two criteria: 1) obtaining large amounts of data per participant (thousands of trials),
992 which is necessary to perform robust drift diffusion modelling of choice behavior and
993 obtain reliable EEG spectral power estimates for each of the ten bins of trials that

994 were created within participants, and 2) obtaining data from a sufficient number of
995 participants to leverage across-subject variability in correlational analyses. Thus, we
996 emphasized obtaining many data points per participant relative to obtaining many
997 participants, while still preserving the ability to perform correlations across
998 participants.

999 All participants were included in the signal-detection-theoretical and drift
1000 diffusion modeling analyses (Figure 2). One participant was excluded from the pre-
1001 stimulus alpha analysis (Figures 3 and 4) due to excessive noise (EEG power
1002 spectrum opposite of 1/frequency). One further participant was excluded from the
1003 gamma analyses (Figures 4, 5 and 6) because the liberal-conservative difference in
1004 gamma power in this participant was > 3 standard deviations away from the other
1005 participants.

1006 **Stimuli** Stimuli consisted of a continuous semi-random rapid serial visual
1007 presentation (rsvp) of full screen texture patterns. The texture patterns consisted of
1008 line elements approx. 0.07° thick and 0.4° long in visual angle. Each texture in the
1009 rsvp was presented for 40 ms (i.e. stimulation frequency 25 Hz), and was oriented in
1010 one of four possible directions: 0° , 45° , 90° or 135° . Participants were instructed to
1011 fixate a red dot in the center of the screen. At random inter trial intervals (ITI's)
1012 sampled from a uniform distribution (ITI range 0.3 – 2.2 s), the rsvp contained a fixed
1013 sequence of 25 texture patterns, which in total lasted one second. This fixed
1014 sequence consisted of four stimuli preceding a (non-)target stimulus (orientations of
1015 45° , 90° , 0° , 90° respectively) and twenty stimuli following the (non-)target
1016 (orientations of 0° , 90° , 0° , 90° , 0° , 45° , 0° , 135° , 90° , 45° , 0° , 135° , 0° , 45° , 90° , 45° ,
1017 90° , 135° , 0° , 135° respectively) (see Figure 2A). The fifth texture pattern within the
1018 sequence (occurring from 0.16 s after sequence onset) was either a target or a

1019 nontarget stimulus. Nontargets consisted of either a 45° or a 135° homogenous
1020 texture, whereas targets contained a central orientation-defined square of 2.42°
1021 visual angle, thereby consisting of both a 45° and a 135° texture. 50% of all targets
1022 consisted of a 45° square and 50% of a 135° square. Of all trials, 75% contained a
1023 target and 25% a nontarget. Target and nontarget trials were presented in random
1024 order. To avoid specific influences on target stimulus visibility due to presentation of
1025 similarly or orthogonally oriented texture patterns temporally close in the cascade, no
1026 45° and 135° oriented stimuli were presented directly before or after presentation of
1027 the target stimulus. All stimuli had an isoluminance of 72.2 cd/m². Stimuli were
1028 created using MATLAB (The Mathworks, Inc., Natick, MA, USA) and presented using
1029 Presentation (Neurobehavioral systems, Inc., Albany, CA, USA).

1030 **Experimental design** The participants' task was to detect and actively report targets
1031 by pressing a button using their right hand. Targets occasionally went unreported,
1032 presumably due to constant forward and backward masking by the continuous
1033 cascade of stimuli and unpredictability of target timing (Fahrenfort, Scholte, &
1034 Lamme, 2007). The onset of the fixed order of texture patterns preceding and
1035 following (non-)target stimuli was neither signaled nor apparent.

1036 At the beginning of the experiment, participants were informed they could
1037 earn a total bonus of EUR 30, -, on top of their regular pay of EUR 10, - per hour or
1038 course credit. In two separate conditions within each session of testing, we
1039 encouraged participants to use either a conservative or a liberal bias for reporting
1040 targets using both aversive sounds as well as reducing their bonus after errors. In
1041 the conservative condition, participants were instructed to only press the button
1042 when they were relatively sure they had seen the target. The instruction on screen
1043 before block onset read as follows: "Try to detect as many targets as possible. Only

1044 press when you are relatively sure you just saw a target.” To maximize effectiveness
1045 of this instruction, participants were told the bonus would be diminished by ten cents
1046 after a false alarm. During the experiment, a loud aversive sound was played after a
1047 false alarm to inform the participant about an error. During the liberal condition,
1048 participants were instructed to miss as few targets as possible. The instruction on
1049 screen before block onset read as follows: “Try to detect as many targets as
1050 possible. If you sometimes press when there was nothing this is not so bad”. In this
1051 condition, the loud aversive sound was played twice in close succession whenever
1052 they failed to report a target, and three cents were subsequently deducted from their
1053 bonus. The difference in auditory feedback between both conditions was included to
1054 inform the participant about the type of error (miss or false alarm), in order to
1055 facilitate the desired bias in both conditions. After every block, the participant’s score
1056 (number of missed targets in the liberal condition and number of false alarms in the
1057 conservative condition) was displayed on the screen, as well as the remainder of the
1058 bonus. After completing the last session of the experiment, every participant was
1059 paid the full bonus as required by the ethical committee.

1060 Participants performed six blocks per session lasting ca. nine minutes each.
1061 During a block, participants continuously monitored the screen and were free to
1062 respond by button press whenever they thought they saw a target. Each block
1063 contained 240 trials, of which 180 target and 60 nontarget trials. The task instruction
1064 was presented on the screen before the block started. The condition of the first block
1065 of a session was counterbalanced across participants. Prior to EEG recording in the
1066 first session, participants performed a 10-minute practice run of both conditions, in
1067 which visual feedback directly after a miss (liberal condition) or false alarm
1068 (conservative) informed participants about their mistake, allowing them to adjust their

1069 decision bias accordingly. There were short breaks between blocks, in which
1070 participants indicated when they were ready to begin the next block.

1071 **Behavioral analysis** We calculated each participant's criterion c (Green & Swets,
1072 1966) across the trials in each condition as follows:

$$c = -\frac{1}{2} [Z(\text{Hit-rate}) + Z(\text{FA-rate})]$$

1073 where hit-rate is the proportion target-present responses of all target-present trials,
1074 false alarm (FA)-rate is the proportion target-present responses of all target-absent
1075 trials, and $Z(\dots)$ is the inverse standard normal distribution. Furthermore, we
1076 calculated objective sensitivity measure d' using:

1077

$$d' = Z(\text{Hit-rate}) - Z(\text{FA-rate})$$

1078

1079 as well as by subtracting hit and false alarm rates. Reaction times (RTs) were
1080 measured as the duration between target onset and button press.

1081 **Drift diffusion modeling of choice behavior** In order to be detected, the 40 ms-
1082 duration figure-ground targets used in our study undergo a process in visual cortex
1083 called figure-ground segregation. This process has been well characterized in man
1084 and monkey (Fahrenfort, Scholte, & Lamme, 2008; Lamme, 1995; Lamme, Zipser, &
1085 Spekreijse, 2006; Supèr, Spekreijse, letters, 2003, 2003), and results from recurrent
1086 processing to extract the surface region in visual cortex. Figure-ground segregation
1087 is known to extend far beyond the mere presentation time of the stimulus, thus
1088 providing a plausible neural basis for the evidence accumulation process. Further, a
1089 central assumption of the drift diffusion model is that the process of evidence

1090 accumulation is gradual, independent of whether sensory input is momentary.
1091 Indeed, the DDM was initially developed to explain reaction time distributions during
1092 memory retrieval, in which evidence accumulation must occur through retrieval of a
1093 memory trace within the brain, in the complete absence of external stimulus at the
1094 time of the decision (Ratcliff, 1978). Our observed RT distributions show the typical
1095 features that occur across many different types of decision and memory tasks, which
1096 the DDM is so well able to capture, including a sharp leading edge and a long tail of
1097 the distributions (see Figure 2-supplement 3). The success of the DDM in fitting
1098 these data is consistent with previous work (e.g. Ratcliff (2006)) and might reflect the
1099 fact that observers modulate the underlying components of the decision process also
1100 when they do not control the stimulus duration (Kiani, Hanks, & Shadlen, 2008).

1101 We fitted the drift diffusion model to our behavioral data for each subject
1102 individually, and separately for the liberal and conservative conditions. We fitted the
1103 model using a G square method based on quantile RT's (RT cutoff, 200 ms, for
1104 details, see Ratcliff et al. (2016)), using a modified version of the HDDM 0.6.0
1105 package (Wiecki, Sofer, & Frank, 2013). The RT distributions for target-present
1106 responses were represented by the 0.1, 0.3, 0.5, 0.7 and 0.9 quantiles, and, along
1107 with the associated response proportions, contributed to G square. In addition, a
1108 single bin containing the number of target-absent responses contributed to G square.
1109 Fitting the model to RT distributions for target-present and target-absent choices
1110 (termed 'stimulus coding' in Wiecki et al. (2013)), as opposed to the more common
1111 fits of correct and incorrect choice RT's (termed 'accuracy coding' in Wiecki et al.
1112 (2013)), allowed us to estimate parameters that could have induced biases in
1113 subjects' behavior.

1114 Parameter recovery simulations showed that letting both the starting point of
1115 the accumulation process and drift bias (an evidence-independent constant added to
1116 the drift toward one or the other bound) free to vary with experimental condition is
1117 problematic for data with no explicit target-absent responses (data not shown). Thus,
1118 to test whether shifts in drift bias or starting point underlie bias we fitted three
1119 separate models. In the first model ('fixed model'), we allowed only the following
1120 parameters to vary between the liberal and conservative condition: (i) the mean drift
1121 rate across trials; (ii) the separation between both decision bounds (i.e., response
1122 caution); and (iii) the non-decision time (sum of the latencies for sensory encoding
1123 and motor execution of the choice). Additionally, the bias parameters starting point
1124 and drift bias were fixed for the experimental conditions. The second model ('starting
1125 point model') was the same as the fixed model, except that we let the starting point
1126 of the accumulation process vary with experimental condition, whereas the drift bias
1127 was kept fixed for both conditions. The third model ('drift bias model') was the same
1128 as the fixed model, except that we let the drift bias vary with experimental condition,
1129 while the starting point was kept fixed for both conditions. We used Bayesian
1130 Information Criterion (BIC) to select the model which provided the best fit to the data
1131 (Neath & Cavanaugh, 2012). The BIC compares models based on their maximized
1132 log-likelihood value, while penalizing for the number of parameters.

1133 **Distinguishing DDM drift bias and drift rate** In our task, only target-present
1134 responses were coupled to a behavioral response (button-press), so we could
1135 measure reaction times only for these responses, whereas reaction times for target-
1136 absent responses remained implicit. Thus, in our fitting procedure, the RT
1137 distributions for target-present responses were represented by the 0.1, 0.3, 0.5, 0.7
1138 and 0.9 quantiles, and, along with the associated response proportions, contributed

1139 to G square. In addition, a single bin containing the number of target-absent
1140 responses contributed to G square. It has been shown that such a diffusion model
1141 with an implicit (no response) boundary can be fit to data with almost the same
1142 accuracy as fitting the two-choice model to two-choice data (Ratcliff et al., 2016). In a
1143 diffusion model with an implicit (no response) boundary, both an increase in drift rate
1144 and drift criterion would predict faster target-present responses. However, the key
1145 distinction is that an increase in drift additionally predicts more correct responses (for
1146 both target-present and target-absent responses), and an increase in drift criterion
1147 shifts the relative fraction of target-present and target-absent responses (decision
1148 bias). Because a single bin containing the number of target-absent responses
1149 contributed to G square, our fitting procedure can distinguish between decision bias
1150 versus drift rate.

1151 **EEG recording** Continuous EEG data were recorded at 256 Hz using a 48-channel
1152 BioSemi Active-Two system (BioSemi, Amsterdam, the Netherlands), connected to a
1153 standard EEG cap according to the international 10-20 system. Electrooculography
1154 (EOG) was recorded using two electrodes at the outer canthi of the left and right
1155 eyes and two electrodes placed above and below the right eye. Horizontal and
1156 vertical EOG electrodes were referenced against each other, two for horizontal and
1157 two for vertical eye movements (blinks). We used the Fieldtrip toolbox (Oostenveld,
1158 Fries, Maris, & Schoffelen, 2011) and custom software in MATLAB R2016b (The
1159 Mathworks Inc., Natick, MA, USA) to process the data (see below). Data were re-
1160 referenced to the average voltage of two electrodes attached to the earlobes.

1161 **Trial extraction and preprocessing** We extracted trials of variable duration from 1
1162 s before target sequence onset until 1.25 after button press for trials that included a
1163 button press (hits and false alarms), and until 1.25 s after stimulus onset for trials

1164 without a button press (misses and correct rejects). The following constraints were
1165 used to classify (non-)targets as detected (hits and false alarms), while avoiding the
1166 occurrence of button presses in close succession to target reports and button
1167 presses occurring outside of trials: 1) A trial was marked as detected if a response
1168 occurred within 0.84 s after target onset; 2) when the onset of the next target
1169 stimulus sequence started before trial end, the trial was terminated at the next trial's
1170 onset; 3) when a button press occurred in the 1.5 s before trial onset, the trial was
1171 extracted from 1.5 s after this button press; 4) when a button press occurred
1172 between 0.5 s before until 0.2 s after sequence onset, the trial was discarded. See
1173 Kloosterman et al. (2015) and Meindertsma et al. (2017) for similar trial extraction
1174 procedures. After trial extraction, channel time courses were linearly detrended and
1175 the mean of every channel was removed per trial.

1176 **Artifact rejection** Trials containing muscle artifacts were rejected from further
1177 analysis using a standard semi-automatic preprocessing method in Fieldtrip. This
1178 procedure consists of bandpass-filtering the trials of a condition block in the 110–125
1179 Hz frequency range, which typically contains most of the muscle artifact activity,
1180 followed by a Z-transformation. Trials exceeding a threshold Z-score were removed
1181 completely from analysis. We used as the threshold the absolute value of the
1182 minimum Z-score within the block, + 1. To remove eye blink artifacts from the time
1183 courses, the EEG data from a complete session were transformed using
1184 independent component analysis (ICA), and components due to blinks (typically one
1185 or two) were removed from the data. In addition, to remove microsaccade-related
1186 artifacts we included two virtual channels in the ICA based on channels Fp1 and
1187 Fp2, which included transient spike potentials as identified using the saccadic
1188 artefact detection algorithm from Hassler et al. (2011). This yielded a total number of

1189 channels submitted to ICA of $48 + 2 = 50$. The two components loading high on
1190 these virtual electrodes (typically with a frontal topography) were also removed.
1191 Blinks and eye movements were then semi-automatically detected from the
1192 horizontal and vertical EOG (frequency range 1–15 Hz; z-value cut-off 4 for vertical;
1193 6 for horizontal) and trials containing eye artefacts within 0.1 s around target onset
1194 were discarded. This step was done to remove trials in which the target was not
1195 seen because the eyes were closed. Finally, trials exceeding a threshold voltage
1196 range of 200 μ V were discarded. To attenuate volume conduction effects and
1197 suppress any remaining microsaccade-related activity, the scalp current density
1198 (SCD) was computed using the second-order derivative (the surface Laplacian) of
1199 the EEG potential distribution (Perrin et al., 1989).

1200 **Spectral analysis of EEG power** We used a sliding window Fourier transform
1201 ((Mitra & Pesaran, 1999); step size, 50 ms; window length, 400 ms; frequency
1202 resolution, 2.5 Hz) to calculate time-frequency representations (spectrograms) of the
1203 EEG power for each electrode and each trial. We used a single Hann taper for the
1204 frequency range of 3–35 Hz (spectral smoothing, 4.5 Hz, bin size, 1 Hz) and the
1205 multitaper technique for the 36 – 100 Hz frequency range (spectral smoothing, 8 Hz;
1206 bin size, 2 Hz; five tapers). See Kloosterman et al. (2015) and Meindertsma et al.
1207 (2017) for similar settings.

1208 Spectrograms were aligned to the onset of the stimulus sequence containing
1209 the (non)target. Power modulations during the trials were quantified as the
1210 percentage of power change at a given time point and frequency bin, relative to a
1211 baseline power value for each frequency bin (Figure 3). We used as a baseline the
1212 mean EEG power in the interval 0.4 to 0 s before trial onset, computed separately for
1213 each condition. If this interval was not completely present in the trial due to

1214 preceding events (see Trial extraction), this period was shortened accordingly. We
1215 normalized the data by subtracting the baseline from each time-frequency bin and
1216 dividing this difference by the baseline ($\times 100\%$). For the analysis of raw pre-
1217 stimulus power modulations, no baseline correction was applied on the raw scalp
1218 current density values. We focused our analysis of EEG power modulations around
1219 target onsets on those electrodes that processed the visual stimulus. To this end, we
1220 averaged the power modulations or raw power across eleven occipito-parietal
1221 electrodes that showed stimulus-induced responses in the gamma-band range (59–
1222 100 Hz). See Kloosterman et al. (2015) and Meindertsma et al. (2017) for a similar
1223 procedure.

1224 **Condition-related raw EEG power change** To test at which frequencies raw EEG
1225 power differed for the liberal and conservative conditions, we averaged raw power
1226 from 0.8 s up to 0.2 s before trial onset (i.e. up to half the window size used for
1227 spectral analysis, to avoid contamination of post- with pre-stimulus activity (Iemi et
1228 al., 2017)). Then, we took the liberal – conservative difference at each frequency bin
1229 and statistically tested whether and at which frequency bins this signal differed from
1230 zero (Figure 4C) (see Statistical comparisons).

1231 **Response gain model test** To test the predictions of the gain model, we first
1232 averaged activity in the 8–12 Hz range from 0.8 to 0.2 s before trial onset (staying
1233 half our window size from trial onset, to avoid mixing pre- and poststimulus activity,
1234 also see Iemi et al. (2017)), yielding a single scalar alpha power value per trial. If this
1235 interval was not completely present in the trial due to preceding events (see Trial
1236 extraction), this period was shortened accordingly. Trials in which the scalar was > 3
1237 standard deviations away from the participant's mean were excluded. We then
1238 sorted all single-trial alpha values for each participant and condition in ascending

1239 order and assigned them to ten bins of equal size, ranging from weakest to strongest
1240 alpha. Adjacent bin ranges overlapped for 50% to stabilize estimates. Then we
1241 averaged the corresponding gamma modulation of the trials belonging to each bin
1242 (consisting of the average power modulation within 59–100 Hz 0.2 to 0.6 s after trial
1243 onset, see Figure 3). Finally, we averaged across participants and plotted the
1244 median alpha value per bin averaged across participants against gamma
1245 modulation. See Rajagovindan and Ding (2011) for a similar procedure. To
1246 statistically test for the existence of inverted U-shaped relationships between alpha
1247 and gamma, we performed a one-way repeated measures ANOVA on gamma
1248 modulation with factor alpha bin (10 bins) to each condition separately and a two-
1249 way repeated measures ANOVA with factors bin and condition for testing the liberal-
1250 conservative difference (Figure 5F). Given the model prediction of a Gaussian-
1251 shaped relationship between alpha and gamma, we constructed a Gaussian contrast
1252 using the normal Gaussian shape with unit standard deviation (contrast values: -
1253 1000, -991, -825, 295, 2521, 2521, 295, -825, -991, -1000, values were chosen to
1254 sum to zero). For plotting purposes (Figure 5C-F), we computed within-subject error
1255 bars by removing within each participant the mean across conditions from the
1256 estimates.

1257 **Correlation between gamma modulation and drift bias** To link DDM drift bias and
1258 cortical gamma power, we re-fitted the DDM drift bias model while freeing the drift
1259 bias parameter both for each condition as well as for the ten alpha bins, while freeing
1260 the other parameters (drift rate, boundary separation, non-decision time) for each
1261 condition and fixing starting point across conditions. We then used repeated
1262 measures correlation to test whether stronger gamma was associated with stronger
1263 bias. Repeated measures correlation determines the common within-individual

1264 association for paired measures assessed on two or more occasions for multiple
1265 individuals by controlling for the specific range in which individuals' measurements
1266 operate, and correcting the correlation degrees of freedom for non-independence of
1267 repeated measurements obtained from each individual. Specifically, the correlation
1268 degrees of freedom were $14 \text{ participants} \times 10 \text{ observations} - \text{Number of participants}$
1269 $- 1 = 140 - 14 - 1 = 125$. Repeated measures correlation tends to have much
1270 greater statistical power than conventional correlation across individuals because
1271 neither averaging nor aggregation is necessary for an intra-individual research
1272 question. Please see Bakdash and Marusich (2017) for more information. We
1273 assessed the impact of single observations on the correlations by excluding
1274 observations exceeding five times the average Cook's distance of all values within
1275 each condition (five observations for liberal and four for conservative) and
1276 recomputing the correlations.

1277 **Statistical comparisons** We used two-sided permutation tests (10,000
1278 permutations) (Efron & Tibshirani, 1998) to test the significance of behavioral effects
1279 and the model fits. Permutation tests yield $p = 0$ if the observed value falls outside
1280 the range of the null distribution. In these cases, $p < 0.0001$ is reported in the
1281 manuscript. The standard deviation (s.d.) is reported as a measure of spread along
1282 with all participant-averaged results reported in the text. To quantify power
1283 modulations after (non-)target onset, we tested the overall power modulation for
1284 significant deviations from zero. For these tests, we used a cluster-based
1285 permutation procedure to correct for multiple comparisons (Maris & Oostenveld,
1286 2007). For time-frequency representations of power modulation, this procedure was
1287 conducted across all time-frequency bins. For frequency spectra, this procedure was
1288 performed across all frequency bins. To test the existence of inverted-U shaped

1289 relationships between gamma and alpha bins, we conducted repeated measures
1290 ANOVA's and Gaussian shaped contrasts (see section Response gain model test for
1291 details) using SPSS 23 (IBM, Inc.). We used Pearson correlation to test the link
1292 between parameter estimates of the DDM and SDT frameworks and repeated
1293 measures correlation to test the link between gamma power and drift bias (see
1294 previous section).